TABLE 1 Patient characteristics ($n = 300$ with CTDs or primary RP)

Variable	SSc ($n = 187$)	SLE ($n = 92$)	MCTD ($n = 11$)	Primary RP ($n = 10$)
Age, mean (S.D.), years	55.3 (13.8)	40.3 (14.9)	59.5 (16.3)	25.4 (3.1)
Gender (F:M), *n:n*	156:31	86:6	11:0	9:1
Smoking, % (*n/N*)	44.2 (50/163)	25.8 (16/46)	0 (0/11)	0 (0/10)
ANA positivity, % (n/N)	91.4 (167/183)	96.7 (89/92)	100 (10/10)	0 (0)
Anti-Scl-70, % (*n/N*)	31.0 (58/187)	NA	NA	0 (0/10)
Anti-centromere, % (*n/N*)	33.7 (63/187)	NA	9.1 (1/11)	0 (0/10)
Anti-Sm, % (*n/N*)	NA	34.5 (30/87)	9.1 (1/11)	NA
Anti-dsDNA, % (*n/N*)	NA	65.1 (54/83)	0 (0/3)	NA
Anti-U1-RNP, % (*n/N*)	7.5 (14/187)	50.0 (43/86)	100.0 (11/11)	0 (0/10)
Anti-SSA/Ro, % (*n/N*)	7.5 (14/187)	57.8 (52/87)	45.5 (5/11)	NA

Scl-70: topoisomerase I; Sm: Smith; U1-RNP: U1 ribonucleoprotein; *N*: the number of available patients (varies according to the number of available observations); NA: not available.

Dako Immunoglobulins, Copenhagen, Denmark). Cells counterstained with Hoechst 33342 (Invitrogen, Carlsbad, CA, USA) were visualized using a Biozero microscope (Keyence, Itasca, IL, USA).

Capture of cell surface proteins

After cold stimulation (10°C) for the indicated periods (0 min, 30 min, 1 h, 3 h), dHMVECs were washed with pre-warmed (37°C) or precooled (10°C) PBS three times and cell surface proteins were then labelled by biotinylation and pulled down by avidin–agarose resin as described previously [3]. The isolated cell surface proteins were kept at −20°C until use.

iTRAQ analysis

Cell surface proteins described above were digested by trypsin and separately labelled with the iTRAQ reagent (Applied Biosystems, Foster City, CA, USA) as described previously [3]. Briefly, iTRAQ reagents 114–117 were used to label cells without cold stimulation (baseline), cells with cold stimulation at 10°C for 30 min, cells with cold stimulation at 10°C for 1 h and cells with cold stimulation at 10°C for 3 h, respectively. Samples were then pooled and fractionated by strong cation exchange chromatography [3]. Nano liquid chromatography–tandem mass spectrometry (LC-MS/MS) analyses were performed on an LTQ-Orbitrap XL (Thermo Fisher Scientific, Waltham, MA, USA) as described previously [3]. Protein identification and quantification for iTRAQ analysis were carried out using Proteome Discoverer software (version 1.1; Thermo Fisher Scientific) against the Swiss Prot protein database [SwissProt 2010_10 (521 016 sequences)] as described previously [3] with modifications as follows: carbamidomethylation and iTRAQ4plex (Lys, N-terminal) were specified as static modifications, whereas CAMthiopropanoyl (Lys, N-terminal), iTRAQ4plex (Tyr) and oxidation (Met) were specified as variable modifications in the database search. The mass spectrometry raw data and the data of peptide identifications were uploaded to PeptideAtlas (http://www.peptideatlas.org/PASS/PASS00387). Information about the subcellular localization of detected proteins was obtained by using UniprotKB (http://www.uniprot.org/).

Serological proteome analysis

Proteins were extracted from cultured dHMVECs using the Complete Mammalian Proteome Extraction Kit (Calbiochem, La Jolla, CA, USA) and stored at −80°C until use. Two-dimensional electrophoresis and immune blotting analysis using patient or HC sera were performed as previously described [10, 11]. Protein spots in a silver-stained gel, corresponding to positive spots on western blot membranes, were excised from the gel and digested in gel as described previously [17].

Preparation of recombinant human hnRNP-K

Full-length hnRNP-K cDNA was amplified from total cDNA of dHMVEC using KOD-plus (Toyobo, Osaka, Japan) with the following primers: 5′-TGGAAACTGAACAGCCAGAAG AA-3′ (forward) and 5′-GCATTAGAATCCTTCAACATCTG C-3′ (reverse). Full-length hnRNP-K cDNA was subcloned into a pET28 vector (Novagen, Madison, WI, USA), resulting in expression of hnRNP-K with a 6 × His tag. The DNA sequence was confirmed using the ABI Prism 3130XL Genetic Analyzer (Applied Biosystems). Recombinant protein was produced in *Escherichia coli* as described previously [10, 11].

ELISA

The ELISA assay was performed using MaxiSorp plates (Nunc A/S, Roskilde, Denmark) coated with 1 μg/well of recombinant human full-length hnRNP-K protein. After dilution (1:500) with *E. coli* cell lysates to block the non-specific reactivity of sera with bacterial proteins, sera were incubated with plate-bound hnRNP-K for 1 h, followed by detection of antigen–antibody complexes by horseradish peroxidase (HRP)-conjugated rabbit anti-human IgG (Dako, Carpinteria, CA, USA) as described previously [10, 11]. Optical density (OD) was read at 450 nm on a Model 680 Microplate Reader (Bio-Rad Laboratories, Hercules, CA, USA). The antibody titre was expressed using arbitrary binding units calculated

Downloaded from http://rheumatology.oxfordjournals.org/ at Osaka University on September 9, 2014

according to the following formula: binding units of sample = [OD_{sample}/(mean $OD_{HC\ sera}$ + 3 S.D.$_{HC\ sera}$)] × 100. Based on this formula, 100 binding units was used as the cut-off point.

Western blot analysis

Extracted proteins were subjected to western blot analysis as previously described [18] with the following antibodies: serum at 1:200 dilution; anti-hnRNP-K (1:500 dilution; Cell Signaling Technology, Danvers, MA, USA); anti-VE-cadherin (1:500 dilution; BD Transduction Laboratories, San Jose, CA, USA); anti-glyceraldehyde-3-phosphate dehydrogenase (GAPDH; 1:1000 dilution; Santa Cruz Biotechnology, Dallas, TX, USA), followed by rabbit anti-human IgG, donkey anti-rabbit or sheep anti-mouse HRP-conjugated secondary antibodies (1:5000 dilution; GE Healthcare, Piscataway, NJ, USA) and visualized with Western Lightning Plus ECL reagent (Perkin-Elmer, Boston, MA, USA).

Fluorescence-activated cell sorting

After stimulation, cells fixed with 4% paraformaldehyde were incubated with rabbit anti-human hnRNP-K antibody at 1:100 dilution and labelled with FITC-conjugated goat anti-rabbit immunoglobulin (BD Biosciences, San Jose, CA, USA). Normal rabbit IgG was used as a control. Stained cells were analysed using a FACS Canto II cytometer (Becton-Dickinson, Mountain View, CA, USA) and the results were analysed using FlowJo software (TreeStar, Ashland, OR, USA).

Statistical analysis

Continuous variables are expressed as mean (S.D.) and proportions were used for categorical variables. Means were compared with Student's *t*-test, highly skewed distributions were compared using the Mann–Whitney *U* test and proportions were compared using Fisher's exact test. Differences between groups were compared using the Kruskall–Wallis test followed by Steel's test. The data were entered and analysed using Excel statistical software (Microsoft, Redmond, WA, USA). Significance was defined as $P < 0.05$.

Results

Cold-induced autoimmune reactions on the cell surface

To determine whether cold can affect autoimmune reactions on the surface of vascular endothelial cells, non-permeabilized dHMVECs pretreated with or without cold stimulation were incubated with sera from patients with RP secondary to SSc or HCs. By indirect immunofluorescence staining using sera from patients, cell surface immunoreactivity was strongly induced in cold-stimulated dHMVECs (eight of nine patients with SSC-related RP; Fig. 1), but not in unstimulated cells. In contrast, no distinct immunostaining was observed in cold-stimulated or unstimulated cells when incubated with sera from HCs ($n = 3$; Fig. 1). These results indicate that pretreatment of dHMVECs with cold is critical in inducing the interaction between cell surface autoantigens and sera from patients.

FIG. 1 Indirect immunofluorescence staining

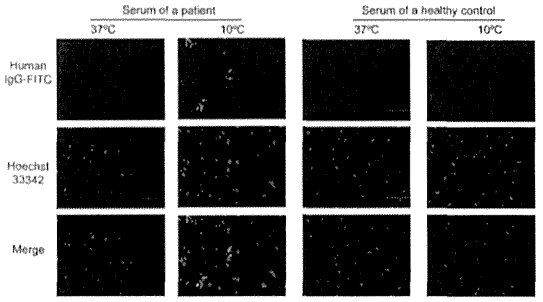

Non-permeabilized cultured dHMVECs with or without cold stimulation were incubated with sera (1:500 dilution) from patients with SSc-related secondary RP ($n = 9$) or healthy controls ($n = 3$) (×100 magnification). Representative images are shown here. FITC-conjugated rabbit anti-human IgG (green); Hoechst 33342 (blue); bar: 100 μm. dHMVECs: dermal human microvascular endothelial cells.

Identification of cold-induced surface proteome alterations in dHMVECs by iTRAQ analysis

The results above suggest that proteins including autoantigens in dHMVECs might be exposed to the cell surface in response to cold stimulation. Therefore we next investigated cold-induced cell surface proteome alterations in dHMVECs. Cells were stimulated with cold (10°C for 0 min, 30 min, 1 h and 3 h) and cell surface proteins enriched by a biotinylation-based approach were quantitatively analysed by iTRAQ technology using nano LC-MS/MS analysis. As listed in supplementary Table S1, available at *Rheumatology* Online, 1581 proteins were identified. According to the annotation from UniprotKB, 451 proteins (28.5%) are located mainly in the plasma membrane, 503 proteins (31.8%) in the cytoplasm, 238 proteins (15.1%) in the nucleus and the remaining proteins (24.6%) in other subfractions such as the mitochondrion and the endoplasmic reticulum. The expression of ~50% of the proteins increased >2-fold after cold stimulation at 10°C for 3 h (see supplementary Table S1, available at *Rheumatology* Online). The top 30 highly increased proteins are listed in Table 2.

Identification of autoantigens by SERPA in patients with secondary RP

We then used a SERPA approach to screen autoantigens associated with secondary RP. At first, proteins from dHMVEC lysates were separated on two-dimensional gels and were visualized by silver staining (Fig. 2A) or were transferred to membranes for immunoblotting. These membranes were incubated with sera from nine

Downloaded from http://rheumatology.oxfordjournals.org/ at Osaka University on September 9, 2014

TABLE 2 List of differentially expressed proteins on the cell surface of dHMVECs after cold stimulation

Accession	Protein name	0.5 h	1 h	3 h
Q96RS6	NudC domain-containing protein 1	3.25	4.24	6.18
P10301	Ras-related protein R-Ras	1.35	3.90	5.95
Q92797	Symplekin	2.94	3.81	5.54
Q643R3	Lysophospholipid acyltranferase LPCAT4	3.06	3.00	5.45
Q99808	Equilibrative nucleoside transporter 1	2.62	3.69	5.21
Q9Y6I9	Testis-expressed sequence 264 protein	2.66	4.11	5.12
Q8TEQ6	Gem-associated protein 5	4.71	6.03	5.08
Q2TAL8	Glutamine-rich protein 1	3.03	4.56	4.99
Q08379	Golgin subfamily A member 2	2.41	4.10	4.74
P49916	DNA ligase 3	2.52	2.94	4.74
P35659	Protein DEK	2.04	3.65	4.67
O60264	SWI/SNF-related matrix-associated actin-dependent regulator of chromatin subfamily A member 5	1.87	4.38	4.52
P60709	Actin, cytoplasmic 1	3.03	3.67	4.28
P55265	Double-stranded RNA-specific adenosine deaminase	2.22	3.86	4.27
Q16643	Drebrin	2.60	3.75	4.24
Q6DD88	Atlastin-3	2.09	3.83	4.14
P29966	Myristoylated alanine-rich C-kinase substrate	1.89	3.61	4.10
Q9ULT8	E3 ubiquitin-protein ligase HECTD1	1.74	3.63	4.08
P61019	Ras-related protein Rab-2A	2.04	3.63	4.03
P61978	hnRNP-K	2.12	3.75	4.03
P01112	GTPase HRas	1.68	2.01	3.95
Q07666	KH domain-containing, RNA-binding, signal transduction-associated protein 1	1.74	3.54	3.92
Q9NZ01	Trans-2,3-enoyl-CoA reductase	1.77	2.08	3.89
Q9NQW6	Actin-binding protein anillin	3.78	5.01	3.86
O00483	NADH dehydrogenase [ubiquinone] 1 alpha subcomplex subunit 4	2.12	2.94	3.86
Q9NP72	Ras-related protein Rab-18	1.96	3.20	3.83
O94901	Protein unc-84 homolog A	2.04	2.77	3.79
P38646	Stress-70 protein, mitochondrial	1.83	3.39	3.76
Q96S97	Myeloid-associated differentiation marker	2.49	3.10	3.75
P49585	Choline-phosphate cytidylyltransferase A	2.68	3.62	3.74

Values are shown as relative expression levels (at 10°C for 0.5, 1 and 3 h) compared with baseline (at 37°C). dHMVECs: dermal human microvascular endothelial cells; hnRNP-K: heterogeneous nuclear ribonucleoprotein K.

patients with RP secondary to SSc (Fig. 2B) or three HCs (Fig. 2C). Six specific spots, which were recognized by sera from >75% of patients, but not by those from HCs, were selected (Fig. 2B). Proteins extracted from the corresponding spots on the silver-stained gel (Fig. 2A) were then subjected to LC-MS/MS analysis and candidate autoantigens were identified by a database search as detailed in Fig. 2D. Among identified candidates, hnRNP-K, a member of the nuclear proteins involved in nucleic acid metabolism [19], was also found in the list of increased proteins on the cell surface under cold stimulation (Table 2), suggesting that hnRNP-K might be a cold-related autoantigen in patients with secondary RP.

Cell surface expression of hnRNP-K under cold stimulation was confirmed by western blot and FACS analysis

The hnRNP proteins are among the most abundant proteins in the nucleus [20]. Indeed, hnRNP-K in dHMVECs under physiological culture conditions was stained intensely in the nucleus by immunofluorescence analysis (see supplementary Fig. S1A and B, available at *Rheumatology* Online). Cold stimulation (10°C for 3 h) induced extranuclear localization of hnRNP-K (see supplementary Fig. S1C and D, available at *Rheumatology* Online), which was nonetheless overwhelmed by intensive staining of nuclear hnRNP-K. To investigate further the appearance of hnRNP-K on the cell surface after cold stimulation, we next performed western blot and FACS analysis. By western blot analysis using concentrated cell surface proteins, hnRNP-K clearly increased in dHMVECs after cold stimulation, but VE-cadherin did not (Fig. 3A). In contrast, the expression level of total hnRNP-K was found to be unchanged during cold stimulation, suggesting that hnRNP-K was not newly synthesized after cold stimulation (Fig. 3A). By FACS analysis, cold-induced expression of hnRNP-K on the cell surface was further confirmed (Fig. 3B). These results collectively suggest that hnRNP-K is a protein that translocates to the cell surface on cold stimulation.

Downloaded from http://rheumatology.oxfordjournals.org/ at Osaka University on September 9, 2014

FIG. 2 Identification of autoantigens by SERPA

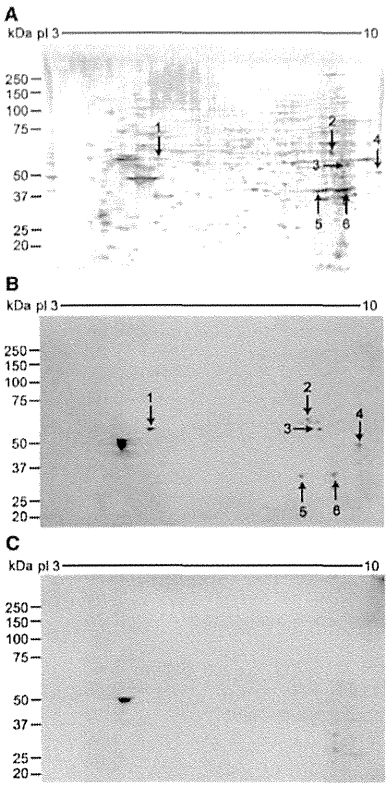

D

no.	Access	Identified protein	Mw(kDa)	PI	Coverage(%)
1	P48643	T-complex protein 1 subunit epsilon	59.63	5.66	30.13
	P61978	Heterogeneous nuclear ribonucleoprotein K	50.94	5.54	19.44
	P10809	60 kDa heat shock protein, mitochondrial	61.92	5.87	16.40
	Q13283	Ras GTPase-activating protein-binding protein 1	52.13	5.52	18.03
	Q92769	Histone deacetylase 2	55.33	5.91	13.11
	Q9H0R6	Glutamyl-tRNA(Gln) amidotransferase subunit A homolog	57.42	5.68	11.55
	Q05682	Caldesmon	93.19	5.67	3.15
	O15460	Prolyl 4-hydroxylase subunit alpha-2	60.86	5.71	4.11
	Q9UN86	Ras GTPase-activating protein-binding protein 2	54.09	5.55	5.19
2	P29401	Transketolase	67.83	7.66	8.19
	P49748	Very long-chain specific acyl-CoA dehydrogenase, mitochondrial	70.35	8.75	4.27
	Q92804	TATA-binding protein-associated factor 2N	61.79	8.02	7.77
3	P14618	Pyruvate kinase isozymes M1/M2	57.90	7.84	25.05
	P50991	T-complex protein 1 subunit delta	57.89	7.83	11.13
	Q14554	Protein disulfide-isomerase A5	59.56	7.91	11.75
	Q99832	T-complex protein 1 subunit eta	59.33	7.65	11.60
	Q9H078	Caseinolytic peptidase B protein homolog	78.68	9.01	7.64
	P06744	Glucose-6-phosphate isomerase	63.11	8.32	4.30
4	P68104	Elongation factor 1-alpha 1	50.11	9.01	16.45
	P06733	Alpha-enolase	47.14	7.39	9.45
	P55084	Trifunctional enzyme subunit beta, mitochondrial	51.26	9.41	6.12
5	P00338	L-lactate dehydrogenase A chain	36.67	8.27	33.13
	Q14192	Four and a half LIM domains protein 2	32.17	7.55	34.41
	P07355	Annexin A2	38.58	7.75	20.06
	P40926	Malate dehydrogenase, mitochondrial	35.48	8.68	18.05
	P22626	Heterogeneous nuclear ribonucleoproteins A2/B1	37.41	8.95	10.20
	P53597	Succinyl-CoA ligase [GDP-forming] subunit alpha, mitochondrial	36.23	8.79	8.67
	Q16270	Insulin-like growth factor-binding protein 7	29.11	7.90	11.70
6	P04406	Glyceraldehyde-3-phosphate dehydrogenase	36.03	8.46	11.94
	P22626	Heterogeneous nuclear ribonucleoproteins A2/B1	37.41	8.95	10.76
	Q9UKM9	RNA-binding protein Raly	32.44	9.17	8.82
	P23193	Transcription elongation factor A protein 1	33.95	8.38	10.30
	P07355	Annexin A2	38.58	7.75	6.19

(**A**–**C**) Total protein extracts of dHMVECs were separated by two-dimensional PAGE followed by silver staining analysis (**A**) or by western blot analysis with diluted sera from SSc patients with RP (**B**) or from healthy controls (**C**). Arrows and numbers indicate protein spots that were recognized only by the patients' sera. Representative images are shown here. (**D**) List of proteins identified by LC-MS/MS analysis (Mw: molecular weight; pI: isoelectric point). dHMVECs: dermal human microvascular endothelial cells; LC-MS/MS: liquid chromatography–tandem mass spectrometry.

Detection of anti-hnRNP-K antibody in sera from patients with secondary RP by western blot and ELISA analysis

To confirm that hnRNP-K is the autoantigen recognized by sera from patients with secondary RP, full-length recombinant human hnRNP-K protein was prepared and subjected to western blot analysis. As disease controls, SSc patients without RP were intentionally recruited to the study and their sera were investigated. Notably, intense reactivity against recombinant hnRNP-K protein was visualized in sera from SSc patients with RP, but not sera from SSc patients without RP or from HCs (Fig. 3C). This result implies that anti-hnRNP-K antibody is relevant to RP rather than to SSc itself.

We then developed an ELISA system using recombinant hnRNP-K protein to screen anti-hnRNP-K antibody in various CTD patients (SSc, SLE and MCTD) with or without RP and in patients with primary RP (Table 1). As shown in Fig. 3D (top), ELISA analysis revealed that significant elevations of anti-hnRNP-K antibody levels were observed in patients with SSc-, SLE- and MCTD-related RP, but not in patients without RP or those with primary RP compared with HCs (Fig. 3D, top). The prevalence of autoantibodies against hnRNP-K was 26.5% in SSc patients with RP, 42.1% in SLE patients with RP and 40.0% in MCTD patients with RP. In contrast, anti-hnRNP-K positivity was markedly low in CTD patients without RP and was 0% in primary RP patients and HCs (Fig. 3D, top). These results suggest that anti-hnRNP-K antibody is relevant to CTD-related secondary RP rather than to a single CTD.

Of all the CTDs (SSc, SLE and MCTD) in this study, a 30.0% prevalence of anti-hnRNP-K antibody was observed in patients with RP, much higher than that in patients without RP (9.20%, $P = 0.0001$), in patients with primary RP (0%, $P = 0.0314$) or in HCs (0%, $P = 0.0003$) (Fig. 3D, bottom). Anti-hnRNP-K-positive CTD patients had a significantly higher prevalence of RP (88.4%) than

Downloaded from http://rheumatology.oxfordjournals.org/ at Osaka University on September 9, 2014

FIG. 3 Cell surface expression of hnRNP-K after cold stimulation and the presence of anti-hnRNP-K autoantibody in sera from patients with secondary RP

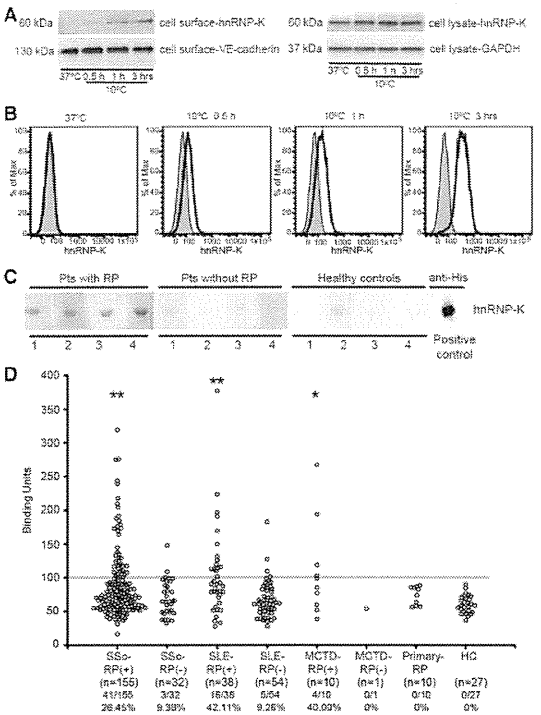

		anti-hnRNP-K	
		Positive	Negative
CTD-RP(+)	n=203	61 (30.0%) †	142 (70.0%)
CTD-RP(-)	n=87	8 (9.20%)	79 (90.8%)
Primary RP	n=10	0 (0%)	10 (100%)
HC	n=27	0 (0%)	27 (100%)

(**A**) Biotinylated surface proteins from dHMVECs incubated at 37°C or 10°C (indicated periods) were precipitated with streptavidin-conjugated agarose beads and analysed by western blot analysis using anti-hnRNP-K. Levels of VE-cadherin surface protein (left panel) and GAPDH expression in total cell lysates (right panel) are shown as controls. (**B**) Cell surface hnRNP-K expression in dHMVECs was analysed by flow cytometry. Shaded histogram indicates staining with control IgG. (**C**) His-tagged recombinant hnRNP-K protein was subjected to western blot analysis using diluted sera from SSc patients with RP, without RP and healthy controls or with anti-6 × His antibody. (**D**) (Top) Serum anti-hnRNP-K antibody levels in indicated CTD patients (with or without RP), primary RP patients and healthy controls were determined by ELISA using recombinant human hnRNP-K. The *y*-axis denotes binding units. The solid horizontal line indicates the positive cut-off limit as described in Materials and methods. Note that this cohort contains a relatively high number of SSc without RP patients and SLE with RP patients, because those patients were intentionally recruited to this study. $^{*}P < 0.05$, $^{**}P < 0.01$ *vs* HCs. (Bottom) Anti-hnRNP-K positivity in patients is summarized. CTD patients are combined here. Values are the number (%) of patients. †$P = 0.00001$ *vs* CTD-RP(−), $P = 0.0314$ *vs* primary RP, $P = 0.0001$ *vs* HCs by Fisher's exact test.
dHMVECs: dermal human microvascular endothelial cells; hnRNP-K: heterogeneous nuclear ribonucleoprotein K; GAPDH: glyceraldehyde-3-phosphate dehydrogenase.

anti-hnRNP-K-negative patients (64.3%, $P = 0.0001$; Table 3). Anti-hnRNP-K antibody showed no correlation with age, gender, smoking or antibodies to U1 ribonucleoprotein (U1-RNP), centromere or SSA/Ro in CTD patients (Table 3). In addition, anti-hnRNP-K showed no correlation with autoantibodies against topoisomerase I (Scl-70) in SSc patients or those against dsDNA or Sm in SLE patients (data not shown). Thus anti-hnRNP-K antibody might be a novel class of biomarker for a subgroup of patients with CTD-related secondary RP.

Discussion

Environmental factors are implicated in the pathogenesis of autoimmune diseases. Previously translocation of intracellular autoantigens to the cell surface was described in ultraviolet radiation-stimulated keratinocytes [21–23]. In the present study, using comprehensive proteomics approaches, we identified hnRNP-K as a novel autoantigen that translocates to the cell surface of dHMVECs after cold stimulation. ELISA analysis revealed that anti-hnRNP-K antibody was significantly elevated in patients with RP secondary to CTDs, but not in patients with primary RP. Thus our data imply hnRNP-K is a putative secondary RP-associated autoantigen that is exposed on the cell surface by cold stimulation.

iTRAQ analysis indicated that cold stimulation in dHMVECs could induce cell surface expression of a variety of proteins, including intracellular proteins, without an overt effect on cell viability, as seen by trypan blue exclusion assay (data not shown). Previous lines of evidence indicate that cytoplasmic and nuclear proteins can reach the cell surface by Golgi-independent non-conventional transport pathways [24–26]. However, it is unknown how cold stimulation induces the translocation of hnRNP-K and other intracellular proteins. Further study is currently under way in our laboratory.

Among many up-regulated proteins identified by iTRAQ analysis, hnRNP-K was the only protein simultaneously identified by SERPA screening. However, our study does not exclude the possibility that there remain other cold-associated autoantigens among these proteins. In particular, since the SERPA approach has limitations in detecting native antigens, antibodies that recognize only native-form autoantigens might have been missed in our study. A screening strategy other than SERPA is necessary to clarify this issue.

hnRNP-K is a 464 amino acid nuclear protein with three K homology domains that mediate DNA and RNA binding [27]. Autoantibodies to hnRNP-K have previously been detected in sera from patients with aplastic anaemia and

Downloaded from http://rheumatology.oxfordjournals.org/ at Osaka University on September 9, 2014

TABLE 3 Basic information of 290 patients with CTDs according to the presence of anti-hnRNP-K antibodies

Variable	Positive ($n = 69$)	Negative ($n = 221$)	*P* value*
Age, mean (S.D.), years	52.4 (15.6)	53.3 (15.4)	0.3613
Gender (F:M), *n:n*	61:8	192:29	0.8383
Smoking, % (*n/N*)	18.9 (10/53)	31.6 (56/177)	0.0841
RP, % (*n*)	88.4 (61)	64.3 (142)	0.0001
ANA positivity, % (*n/N*)	94.0 (63/67)	93.1 (203/218)	1.0000
Anti-U1-RNP, % (*n/N*)	26.5 (18/68)	23.1 (50/166)	0.6255
Anti-SSA/Ro positivity, % (*n/N*)	27.9 (19/68)	23.6 (52/220)	0.5202

*Univariate analysis using the Mann–Whitney U test or Fisher's exact test. *N*: the number of available patients (varies according to the number of available observations). hnRNP-K: heterogeneous nuclear ribonucleoprotein K.

RA (31% and 24%, respectively), although the co-morbidity of RP in these patients was not described in this report [28]. Autoantibodies to other hnRNPs such as hnRNP-H1 [29], -B1 and -F [30] have also been reported as possible diagnostic markers of CTDs, but their relevance to RP has not been examined.

Although anti-hnRNP-K antibody was identified initially using sera from patients with SSc-related RP, this autoantibody was also detected in sera from RP patients with other CTDs. Notably, anti-hnRNP-K antibody levels in RP patients secondary to SSc, SLE and MCTD were significantly higher than in HCs. In addition, the prevalence of anti-hnRNP-K antibody in SSc patients with RP (26.5%), SLE patients with RP (42.1%) and MCTD patients with RP (40.0%) was markedly higher than in their RP-negative counterparts (9.4%, 9.3% and 0%, respectively) and in primary RP patients (0%). Moreover, anti-hnRNP-K autoantibody was not associated with smoking, which was believed to be a cause of blood vessel narrowing [31], nor with the presence of anti-U1-RNP and ACAs, which are highly related to MCTD and SSc, respectively [32, 33]. Thus these results suggest that anti-hnRNP-K antibody is particularly relevant to CTD-related secondary RP, but not to a single CTD or primary RP. Our findings should be replicated in a larger study.

The pathogenesis of RP likely involves various abnormalities in the vascular, neural and intravascular systems [4]. At present, it remains to be determined whether anti-hnRNP-K autoantibody detected by our ELISA system can bind to hnRNP-K on vascular endothelial cells *in vivo*. In addition, it is unknown whether this autoantibody contributes to the pathogenesis. Because our cohort of patients includes only a limited number of severe RP patients who experienced hospitalization and/or digit loss, it is unknown whether anti-hnRNP-K antibody correlates with the severity of RP. However, it is tempting to speculate that following cold stimulation, anti-hnRNP-K autoantibody may promote antibody-dependent pathogenesis by inducing vascular endothelial damage. As previously reported, anti-endothelial cell antibodies (AECAs) are a heterogeneous group of autoantibodies against various cell surface proteins in endothelial cells and can contribute leucocyte adhesion by inducing adhesion molecules and cytokines in endothelial cells [34–36]. Anti-hnRNP-K antibody may thus be a class of AECA that becomes active under cold stimulation in patients with secondary RP. Further analyses are needed to elucidate the correlation of anti-hnRNP-K autoantibodies with the pathogenesis of secondary RP.

In summary, we provide the first evidence of cold-associated autoantibodies in patients with secondary RP. Anti-hnRNP-K antibody may be a potential biomarker for RP secondary to CTDs. Longitudinal studies are warranted to determine whether the evaluation of anti-hnRNP-K antibody in RP patients may aid in the detection of CTDs in these patients.

Rheumatology key messages

- Cold-associated autoantibody in patients with secondary RP is successfully identified by a proteomic approach.
- hn-RNP-K translocates to the endothelial cell surface upon cold stimulation.
- Anti-hnRNP-K autoantibody may serve as a biomarker for secondary RP.

Acknowledgements

We would like to thank Y. Kanazawa and J. Yamagishi for secretarial assistance and M. Urase and K. Yoshimoto for technical assistance.

Funding: This study was supported by a grant-in-aid for the Program for Promotion of Fundamental Studies in Health Sciences of the National Institute of Biomedical Innovation and a Grant-in-Aid for Research on Biological Markers for New Drug Development (H20-0005) from the Ministry of Health, Labour and Welfare of Japan.

Disclosure statement: The authors have declared no conflicts of interest.

Downloaded from http://rheumatology.oxfordjournals.org/ at Osaka University on September 9, 2014

Supplementary data

Supplementary data are available at *Rheumatology* Online.

References

1 Unwin RD, Griffiths JR, Whetton AD. Simultaneous analysis of relative protein expression levels across multiple samples using iTRAQ isobaric tags with 2D nano LC-MS/MS. Nat Protoc 2010;5:1574–82.

2 Serada S, Fujimoto M, Ogata A *et al*. iTRAQ-based proteomic identification of leucine-rich alpha-2 glycoprotein as a novel inflammatory biomarker in autoimmune diseases. Ann Rheum Dis 2010;69:770–4.

3 Yokoyama T, Enomoto T, Serada S *et al*. Plasma membrane proteomics identifies bone marrow stromal antigen 2 as a potential therapeutic target in endometrial cancer. Int J Cancer 2013;132:472–84.

4 Herrick AL. The pathogenesis, diagnosis and treatment of Raynaud phenomenon. Nat Rev Rheumatol 2012;8:469–79.

5 Bakst R, Merola JF, Franks AG Jr, Sanchez M. Raynaud's phenomenon: pathogenesis and management. J Am Acad Dermatol 2008;59:633–53.

6 Dimant J, Ginzler E, Schlesinger M *et al*. The clinical significance of Raynaud's phenomenon in systemic lupus erythematosus. Arthritis Rheum 1979;22:815–9.

7 Grader-Beck T, Wigley FM. Raynaud's phenomenon in mixed connective tissue disease. Rheum Dis Clin North Am 2005;31:465–81, vi.

8 Maricq HR, Harper FE, Khan MM, Tan EM, LeRoy EC. Microvascular abnormalities as possible predictors of disease subsets in Raynaud phenomenon and early connective tissue disease. Clin Exp Rheumatol 1983;1:195–205.

9 Srivastava R, Aslam M, Kalluri SR *et al*. Potassium channel KIR4.1 as an immune target in multiple sclerosis. N Engl J Med 2012;367:115–23.

10 Serada S, Fujimoto M, Takahashi T *et al*. Proteomic analysis of autoantigens associated with systemic lupus erythematosus: anti-aldolase A antibody as a potential marker of lupus nephritis. Proteomics Clin Appl 2007;1:185–91.

11 He P, Naka T, Serada S *et al*. Proteomics-based identification of alpha-enolase as a tumor antigen in non-small lung cancer. Cancer Sci 2007;98:1234–40.

12 Masi AT. Preliminary criteria for the classification of systemic sclerosis (scleroderma). Subcommittee for scleroderma criteria of the American Rheumatism Association Diagnostic and Therapeutic Criteria Committee. Arthritis Rheum 1980;23:581–90.

13 Tan EM, Cohen AS, Fries JF *et al*. The 1982 revised criteria for the classification of systemic lupus erythematosus. Arthritis Rheum 1982;25:1271–7.

14 Hochberg MC. Updating the American College of Rheumatology revised criteria for the classification of systemic lupus erythematosus. Arthritis Rheum 1997;40:1725.

15 Kasukawa R, Tojo T, Miyawaki S. Preliminary diagnostic criteria for classification of mixed connective tissue disease. In: Kasukawa R, Sharp GC, eds. Mixed Connective Tissue Diseases and Antinuclear Antibodies. Amsterdam, the Netherlands: Elsevier, 1987:41–7.

16 Brennan P, Silman A, Black C *et al*. Validity and reliability of three methods used in the diagnosis of Raynaud's phenomenon. The UK Scleroderma Study Group. Br J Rheumatol 1993;32:357–61.

17 Umegaki-Arao N, Tamai K, Nimura K *et al*. Karyopherin alpha2 is essential for rRNA transcription and protein synthesis in proliferative keratinocytes. PLoS One 2013;8:e76416.

18 Yang L, Serada S, Fujimoto M *et al*. Periostin facilitates skin sclerosis via PI3K/Akt dependent mechanism in a mouse model of scleroderma. PLoS One 2012;7:e41994.

19 Han SP, Tang YH, Smith R. Functional diversity of the hnRNPs: past, present and perspectives. Biochem J 2010;430:379–92.

20 Dreyfuss G, Matunis MJ, Pinol-Roma S, Burd CG. hnRNP proteins and the biogenesis of mRNA. Annu Rev Biochem 1993;62:289–321.

21 Furukawa F, Kashihara-Sawami M, Lyons MB, Norris DA. Binding of antibodies to the extractable nuclear antigens SS-A/Ro and SS-B/La is induced on the surface of human keratinocytes by ultraviolet light (UVL): implications for the pathogenesis of photosensitive cutaneous lupus. J Invest Dermatol 1990;94:77–85.

22 Wang B, Dong X, Yuan Z, Zuo Y, Wang J. SSA/Ro antigen expressed on membrane of UVB-induced apoptotic keratinocytes is pathogenic but not detectable in supernatant of cell culture. Chin Med J 1999;112:512–5.

23 Golan TD, Elkon KB, Gharavi AE, Krueger JG. Enhanced membrane binding of autoantibodies to cultured keratinocytes of systemic lupus erythematosus patients after ultraviolet B/ultraviolet A irradiation. J Clin Invest 1992;90:1067–76.

24 Nickel W, Seedorf M. Unconventional mechanisms of protein transport to the cell surface of eukaryotic cells. Annu Rev Cell Dev Biol 2008;24:287–308.

25 Nickel W, Rabouille C. Mechanisms of regulated unconventional protein secretion. Nat Rev Mol Cell Biol 2009;10:148–55.

26 Nickel W. Pathways of unconventional protein secretion. Curr Opin Biotechnol 2010;21:621–6.

27 Bomsztyk K, Denisenko O, Ostrowski J. hnRNP K: one protein multiple processes. Bioessays 2004;26:629–38.

28 Qi Z, Takamatsu H, Espinoza JL *et al*. Autoantibodies specific to hnRNP K: a new diagnostic marker for immune pathophysiology in aplastic anemia. Ann Hematol 2010;89:1255–63.

29 Van den Bergh K, Hooijkaas H, Blockmans D *et al*. Heterogeneous nuclear ribonucleoprotein h1, a novel nuclear autoantigen. Clin Chem 2009;55:946–54.

30 Op De Beeck K, Maes L, Van den Bergh K *et al*. Heterogeneous nuclear RNPs as targets of autoantibodies in systemic rheumatic diseases. Arthritis Rheum 2012;64:213–21.

Downloaded from http://rheumatology.oxfordjournals.org/ at Osaka University on September 9, 2014

31 D.S.G. Tobacco report: PHS Study Group, after 14-month survey, agrees that smoking is indeed harmful. Science 1964;143:227.

32 Buchanan RR, Riglar AG. The titre of anti-centromere antibodies: its relationship to Raynaud's phenomenon and vascular occlusion. Br J Rheumatol 1989;28:221–6.

33 Furtado RN, Pucinelli ML, Cristo VV, Andrade LE, Sato EI. Scleroderma-like nailfold capillaroscopic abnormalities are associated with anti-U1-RNP antibodies and Raynaud's phenomenon in SLE patients. Lupus 2002;11: 35–41.

34 Carvalho D, Savage CO, Black CM, Pearson JD. IgG antiendothelial cell autoantibodies from scleroderma patients induce leukocyte adhesion to human vascular endothelial cells in vitro. Induction of adhesion molecule expression and involvement of endothelium-derived cytokines. J Clin Invest 1996;97:111–9.

35 Del Papa N, Guidali L, Sironi M *et al.* Anti-endothelial cell IgG antibodies from patients with Wegener's granulomatosis bind to human endothelial cells in vitro and induce adhesion molecule expression and cytokine secretion. Arthritis Rheum 1996;39:758–66.

36 Lin CF, Chiu SC, Hsiao YL *et al.* Expression of cytokine, chemokine, and adhesion molecules during endothelial cell activation induced by antibodies against dengue virus nonstructural protein 1. J Immunol 2005;174:395–403.

Downloaded from http://rheumatology.oxfordjournals.org/ at Osaka University on September 9, 2014

Journal of General Virology (2014), **95**, 2769–2777 DOI 10.1099/vir.0.069336-0

Human herpesvirus 6 gM/gN complex interacts with v-SNARE in infected cells

Akiko Kawabata,[1] Satoshi Serada,[2] Tetsuji Naka[2] and Yasuko Mori[1]

Correspondence
Yasuko Mori
ymori@med.kobe-u.ac.jp

[1]Division of Clinical Virology, Center for Infectious Diseases, Kobe University Graduate School of Medicine, 7-5-1, Kusunoki-cho, Chuo-ku, Kobe 650-0017, Japan

[2]Laboratory of Immune Signal, Division of Biomedical Research, National Institute of Biomedical Innovation, 7-6-8, Saito-Asagi, Ibaraki, Osaka 567-0085, Japan

Received 23 June 2014
Accepted 9 September 2014

Human herpesvirus 6 (HHV-6) glycoprotein M (gM) is an envelope glycoprotein that associates with glycoprotein N (gN), forming the gM/gN protein complex, in a similar manner to the other herpesviruses. Liquid chromatography-MS/MS analysis showed that the HHV-6 gM/gN complex interacts with the v-SNARE protein, vesicle-associated membrane protein 3 (VAMP3). VAMP3 colocalized with the gM/gN complex at the *trans*-Golgi network and other compartments, possibly the late endosome in HHV-6-infected cells, and its expression gradually increased during the late phase of virus infection. Finally, VAMP3 was incorporated into mature virions and may be transported with the gM/gN complex.

INTRODUCTION

Human herpesvirus 6 (HHV-6) belongs to the betaherpesvirus subfamily (Roizmann *et al.*, 1992). HHV-6 isolates can be classified as HHV-6A and HHV-6B (Ablashi *et al.*, 2013) based on genetic and antigenic differences, cell tropism, and pathogenesis (Ablashi *et al.*, 1991; Aubin *et al.*, 1991; Campadelli-Fiume *et al.*, 1993; Chandran *et al.*, 1992; Mori, 2009; Yamanishi *et al.*, 1988).

Herpesviruses encode several glycoproteins on the envelope of viral particles that work for entry, assembly and egress of the virus. Of these, glycoprotein M (gM) is a remarkable envelope glycoprotein as it is conserved among all herpesvirus subfamilies. Most herpesviruses, including herpes simplex virus type-1 (Baines & Roizman, 1991), pseudorabies virus (Dijkstra *et al.*, 1996) and equine herpesvirus 1 (Osterrieder *et al.*, 1996), do not require gM for replication. Marek's disease virus (Tischer *et al.*, 2002) and varicella-zoster virus (Yamagishi *et al.*, 2008) abolish virus growth *in vitro*. However, the gM protein of human cytomegalovirus (HCMV), which belongs to the betaherpesvirus subfamily, is essential for the production of infectious virus (Hobom *et al.*, 2000).

HHV-6 gM is a product of the U72 ORF and comprises 343 aa (Kawabata *et al.*, 2012; Lawrence *et al.*, 1995). Post-infection (p.i.), it is translated into a 47–63 kDa protein that is post-translationally glycosylated (Kawabata *et al.*, 2012). It is a type III transmembrane protein with seven membrane-spanning domains and a C-terminal cytoplasmic tail. HHV-6 gM interacts with the product of the U46 ORF, known as gN, to form a complex for transport to the *trans*-Golgi network (TGN) and endosomal compartments (Kawabata *et al.*, 2012). Finally, the gM/gN complex is incorporated into mature virions. Interestingly, unlike in alpha herpesviruses, HHV-6 gM is essential for virus growth (Kawabata *et al.*, 2012).

To further examine the role of HHV-6A gM during HHV-6 infection, we performed liquid chromatography (LC)-MS/MS analysis to identify the cellular components that interact with the gM/gN complex. The results showed that the gM/gN complex interacts with VAMP3 (vesicle-associated membrane protein 3).

VAMP3 is a v-SNARE (soluble *N*-ethylmaleimide-sensitive factor attachment protein receptor) protein that resides in recycling endosomes and endosome-derived transport vesicles. v-SNARE interacts with SNARE proteins on target membranes (t-SNAREs) to form *trans*-SNARE complexes, which draw the two membranes together and drive membrane fusion (Jahn & Scheller, 2006; Jahn *et al.*, 2003; Rothman, 1994; Söllner *et al.*, 1993). SNAREs are cytoplasmic-oriented type I membrane proteins that play a role in intracellular trafficking mechanisms during exocytosis by forming a complex that facilitates the transient fusion of the vesicular and plasma membrane lipid bilayers (Mohrmann & Sørensen, 2012). This membrane fusion is dependent on the formation of a complex between t-SNARE and v-SNARE proteins (Jahn & Scheller, 2006; Jahn *et al.*, 2003).

VAMP3 is localized to recycling endosomes (McMahon *et al.*, 1993) and plays a role in the fusion of recycling endosomes and the plasma membrane by forming a complex with the surface t-SNARE complex, Stx4/SNAP23 (Hu *et al.*, 2007). The VAMP3/Stx4/SNAP23 SNARE complex mediates the long-loop recycling pathway that delivers recycling endosomes and their cargo to the cell

surface, and plays an important role in regulating the ability of macrophages to effectively adhere and spread on fibronectin (Veale *et al.*, 2011). VAMP3 is also involved in integrin trafficking, cell migration and cell adhesion (Luftman *et al.*, 2009; Tayeb *et al.*, 2005). In addition, it plays a role in the exocytosis of α-granules in platelets (Polgár *et al.*, 2002), as well as in the recycling of endocytosed transferrin receptors to the cell surface (Galli *et al.*, 1994).

Here, we describe the interaction between the gM/gN complex and VAMP3 in HHV-6A-infected cells and discuss the potential for the association between the gM/gN complex and VAMP3 to modify its localization and mediate its incorporation into mature virions.

RESULTS

Identification of cellular proteins interacting with the gM/gN complex

A recent study showed that the cytoplasmic tail of HCMV gM interacts with the cellular protein FIP4, which is a Rab11-GTPase effector protein important for gM/gN trafficking and for accumulation of the envelope glycoprotein complex in the assembly compartment in HCMV-infected cells (Krzyzaniak *et al.*, 2009). To examine the function of HHV-6A gM/gN, we tried to identify the cellular protein(s) that interact with the gM/gN complex. First, gM and gN were cotransfected into 293T cells and gM was immunoprecipitated from the lysates with an anti-gM mAb. Silver staining of gels containing proteins separated from the lysates of the gM/gN-expressing cells revealed several specific bands at approximately 10 kDa; these proteins were not present in the lysates of cells expressing gM alone. One specific band (Fig. 1a, arrowhead) was excised from the gel and subjected to LC-MS/MS analysis. The results of this analysis identified VAMP3 as the interacting protein (Fig. 1b).

To confirm the interaction between VAMP3 and gM/gN, lysates from cells expressing both HA-tagged gM and FLAG-tagged gN were immunoprecipitated with an anti-HA antibody, followed by Western blotting with anti-gM, anti-FLAG or anti-VAMP3 antibodies. As shown in Fig. 1c, VAMP3 was coprecipitated when gM and gN were coexpressed. However, VAMP3 was not coprecipitated when gM or gN was expressed alone. CD63 was not coprecipitated even when gM and gN were coexpressed (Fig. 1c). These results indicate that VAMP3 interacts with the gM/gN complex.

Interaction between gM and VAMP3 in HHV-6A-infected cells

To confirm the interaction between the gM/gN complex and VAMP3 in HHV-6A-infected cells, lysates from HHV-6A-infected HSB-2 cells were immunoprecipitated with an anti-gM mAb or an anti-VAMP3 antibody, followed by Western blotting with anti-gM, anti-VAMP3, anti-CD63 or anti-gB antibodies (Fig. 2). Endogenous VAMP3 coprecipitated with gM and vice versa; gB or endogenous CD63 coprecipitated with neither gM nor VAMP3 (Fig. 2b). These results indicate that gM also interacts with VAMP3 in HHV-6A-infected cells. Interestingly, although gM with a molecular mass of 15 kDa was detected in the lysates of HHV-6A-infected cells, it did not coprecipitate with the anti-VAMP3 antibody.

To examine the cellular localization of gM and VAMP3 in HHV-6A-infected cells, an indirect immunofluorescence assay (IFA) was performed using HHV-6A-infected HSB-2 cells at 96 h p.i. (Fig. 3). Confocal microscopy of HHV-6A-infected HSB-2 cells showed that gM and VAMP3 appear to partially colocalize to the same cellular compartment. In addition, gM and VAMP3 partially colocalized with TGN46, a marker of the TGN (Fig. 3b), and with CD63, a marker of late endosomes and multivesicular bodies (MVB) (Fig. 3a). The expression of endogenous VAMP3 was much lower in uninfected cells than infected cells [Fig. 3a(ii), b(ii)]. These results indicate that VAMP3 may localize with gM to the endosomal compartment in addition to TGN during the late stage of infection. Preimmune serum of guinea pig did not react with either HHV-6A-infected [Fig. 3d(i)] or uninfected cells [Fig. 3d(ii)], although anti-VAMP3 antibody obtained from the same guinea pig reacted with HHV-6A-infected cells [Fig. 3c(i)] but not uninfected cells [Fig. 3c(ii)].

VAMP3 is present in purified HHV-6A virions

Recently, we showed that HHV-6A virions are released through MVBs via the cellular exosomal pathway and that gB and gM are present on exosomes (Mori *et al.*, 2008). To examine whether VAMP3 expressed in HHV-6A-infected cells is present on virions and exosomes, we purified virions from the culture medium of HHV-6A-infected cells. As expected, VAMP3, gM and CD63 were detected by western blotting of the virion fractions (Fig. 4a). Virion fractions were confirmed with the presence of gB (Fig. 4a) and viral DNA (Fig. 4b). In addition, VAMP3 was detected on HHV-6A virions by immunogold labelling electron microscopy analysis [Fig. 4c(i)], but it was rarely detected on virions without primary antibody [Fig. 4c(ii)]. These results indicate that VAMP3 is incorporated into viral particles along with the gM/gN complex.

Intracellular localization of the gM/gN complex and VAMP3 in cells transiently expressing gM/gN

We next examined the intracellular localization of gM, gN and VAMP3 (Fig. 5). When plasmids expressing gM and gN were cotransfected into HeLa cells [Fig. 5a(i)], gM/gN colocalized with endogenous VAMP3 in the perinuclear region. However, when gM was expressed alone, it failed to colocalize with VAMP3 [Fig. 5a(ii)]. Because the gM/gN complex localized to the TGN in HHV-6A-infected cells, we hypothesized that the gM/gN complex would interact with

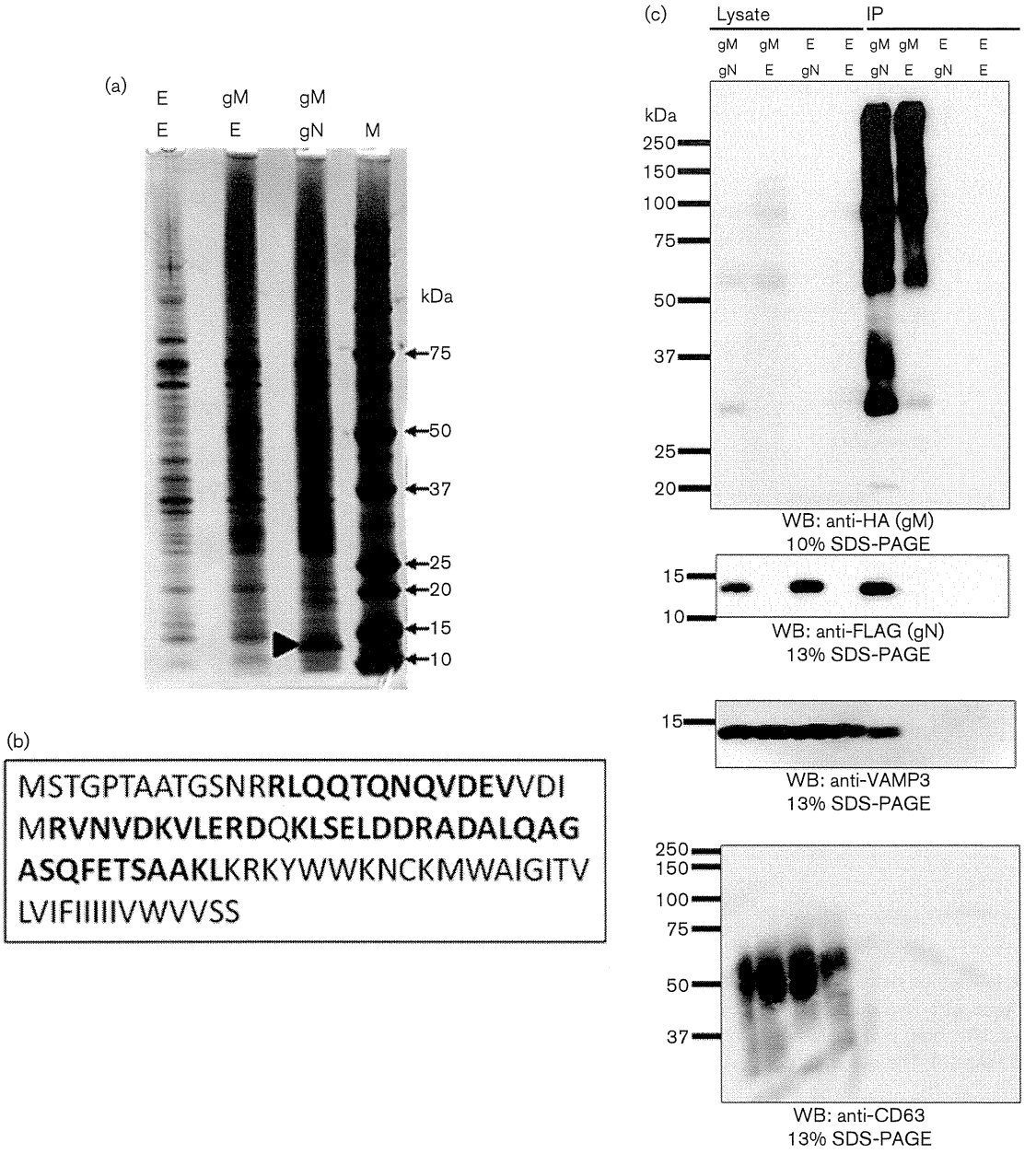

Fig. 1. Interaction between gM/gN and VAMP3. (a) 293T cells were transfected with plasmids expressing HA-tagged gM and FLAG-tagged gN. The cells were lysed with TNE buffer at 72 h post-transfection. The lysates were then immunoprecipitated with an anti-HA Ab specific for gM and visualized by silver staining. The band marked by the arrowhead indicates the protein selected for analysis by LC-MS/MS. (b) Peptide matches to the VAMP3 sequence are shown in bold. (c) 293T cells were transfected with plasmids expressing HA-tagged gM, FLAG-tagged gN, or pCAGGS (negative control). The cells were then lysed with TNE buffer at 72 h post-transfection. The lysates were immunoprecipitated with anti-HA antibody for gM and analysed by Western blotting with anti-HA, anti-FLAG, anti-VAMP3 (BioReagents) or anti-CD63 antibodies. The numbers beside the panels indicate the molecular masses (kDa). WB, Western blotting; E, empty.

VAMP3 at the TGN or a TGN-derived compartment. As expected, when gM was coexpressed with gN, it colocalized with VAMP3 and TGN46 (Fig. 5b); however, this colocalization was not observed when gM was expressed alone [Fig. 5a(ii)]. These results suggest that the interaction between the gM/gN complex and VAMP3 occurs at the TGN or a TGN-derived compartment. Glycoprotein M did not colocalize with CD63 even when gM was coexpressed with gN [Fig. 4c(i)]. Non-specific staining of gM was not seen in these cells [Fig. 5a(iii), b(ii), c(ii)].

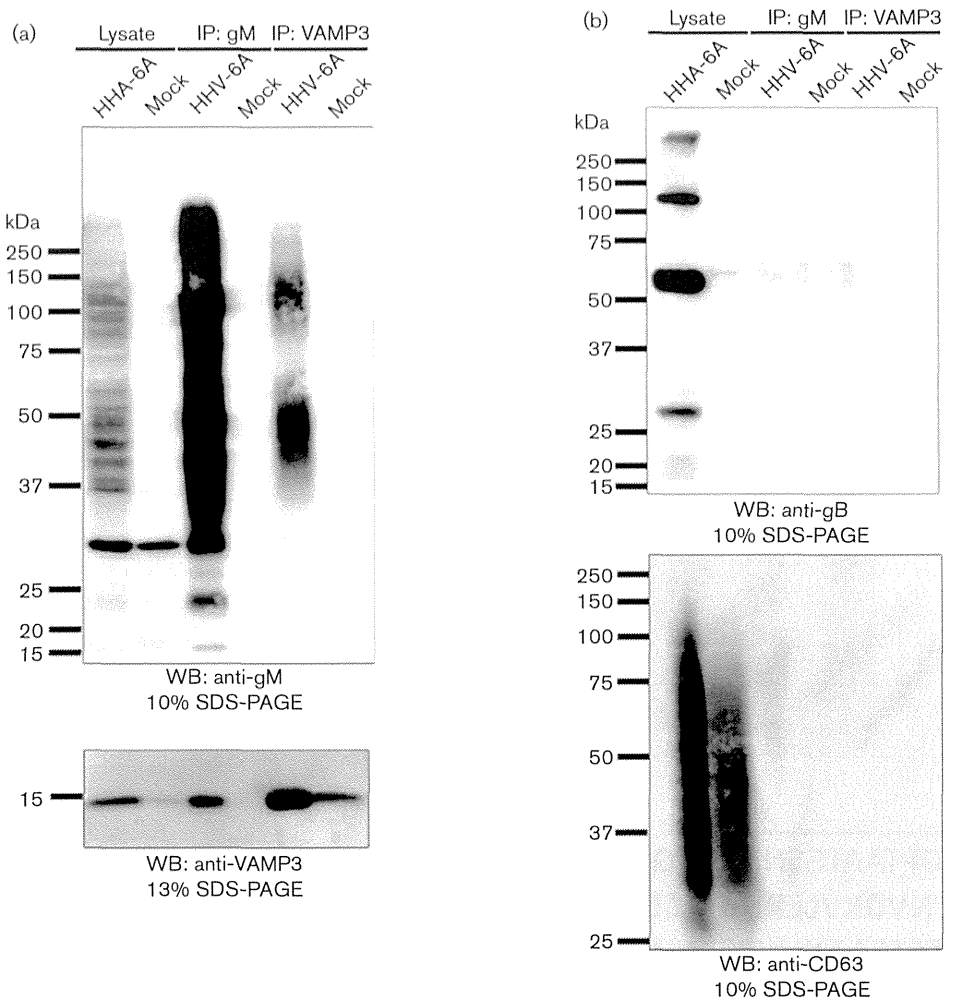

Fig. 2. Interaction between gM and VAMP3 in HHV-6A-infected HSB-2 cells. HHV-6A-infected or mock-infected HSB-2 cells were lysed with TNE buffer at 96 h post-infection. The lysates were immunoprecipitated (IP) with anti-gM mAb or anti-VAMP3 Ab (see Methods) and analysed by Western blotting with anti-gM or anti-VAMP3 (BioReagents) Abs (a), anti-gB Ab or anti-CD63 mAb (b). The numbers beside the panels indicate the molecular masses (kDa). WB, Western blotting.

The kinetics of VAMP3 expression in HHV-6A-infected cells

As shown in Fig. 2, VAMP3 expression in HHV-6A-infected cells was higher than that in mock-infected cells. Therefore, we examined the kinetics of VAMP3 expression in HHV-6A-infected cells. The results in Fig. 6 show that VAMP3 expression increased gradually in the infected cells.

DISCUSSION

Here, we used the transient expression of gM and gN to identify VAMP3 as a cellular molecule that interacts with the HHV-6A gM/gN complex. The interaction between VAMP3 and the gM/gN complex was also confirmed in HHV-6A-infected cells. VAMP3 and gM/gN proteins colocalized at the TGN in cells coexpressing gM and gN, and in HHV-6A-infected cells. This interaction was observed only when gM/gN formed a complex, indicating that the interaction is required for gM/gN complex formation. Previously, we reported that the localization of HHV-6A gM to the TGN was necessary for its interaction with gN (Kawabata *et al.*, 2012). Therefore, the interaction between the gM/gN complex and VAMP3 might also occur at the TGN. It is still not known whether the interaction between VAMP3 and gM requires gM/gN complex formation. Transport of gM to the TGN might be required for this interaction.

VAMP3 also colocalized with CD63, which is a marker of late endosome in HHV-6A-infected cells. In cells transiently expressing gM and gN, however, VAMP3 colocalized with TGN46, but not CD63. This suggests that in infected cells, the localization of VAMP3 may be modified through its interaction with gM/gN, thereby possibly allowing it to localize to the other organelles, such as the late endosome.

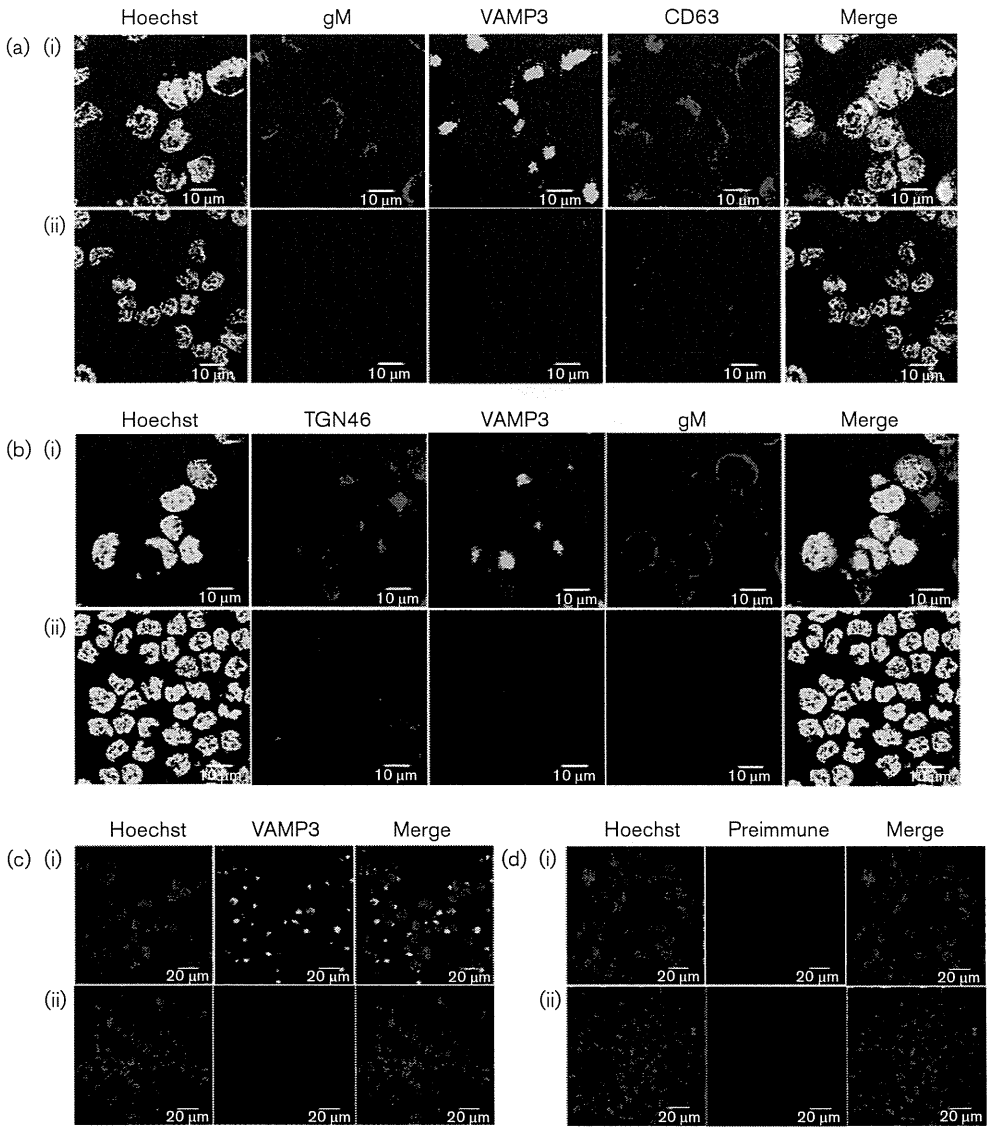

Fig. 3. Colocalization of gM, VAMP3 and CD63, or gM, VAMP3 and TGN46 in HHV-6A-infected cells. HHV-6A-infected [a(i), b(i)] or mock-infected [a(ii), b(ii)] HSB-2 cells were harvested at 96 h post-infection and fixed. The cells were stained with antibodies against VAMP3, gM and CD63 as well as with Hoechst 33258 (a), or VAMP3, gM and TGN46 as well as with Hoechst 33258 (b). Costained areas appear white in the merged panel. Bars, 10 μm. HHV-6A-infected [c(i), d(i)] or mock-infected [c(ii), d(ii)] cells were stained with guinea pig antisera against VAMP3 (c) or preimmune sera obtained from the same guinea pig as well as with Hoechst 33258 (d). Bars, 20 μm.

We also found that VAMP3 was incorporated into virions. As the gM/gN complex is expressed on virions and exosomes, complex-associated VAMP3 would be transported along with the gM/gN complex and then released via the exosomal release pathway (Mori *et al.*, 2008).

Although the function of VAMP3 in HHV-6A-infected cells is not known, its interaction with the gM/gN complex may modify the cellular machinery in infected cells. As VAMP3 is incorporated into virions and exosomes, its primary function (to facilitate membrane fusion) may be lost in infected cells. Overexpression of VAMP3 did not affect HHV-6 growth (data not shown). Several v-SNARE proteins with functions similar to those of VAMP3 have been identified (Borisovska *et al.*, 2005). Therefore, the function of VAMP3 may be redundant in HHV-6A-infected cells. It is still not known whether v-SNAREs, including VAMP3, are required for HHV-6 infection. Further studies will be required to address these questions.

METHODS

Cells and viruses. The HSB-2 T-cell line was cultured in RPMI 1640 medium (Nissui) supplemented with 8 % FBS. Human embryonic

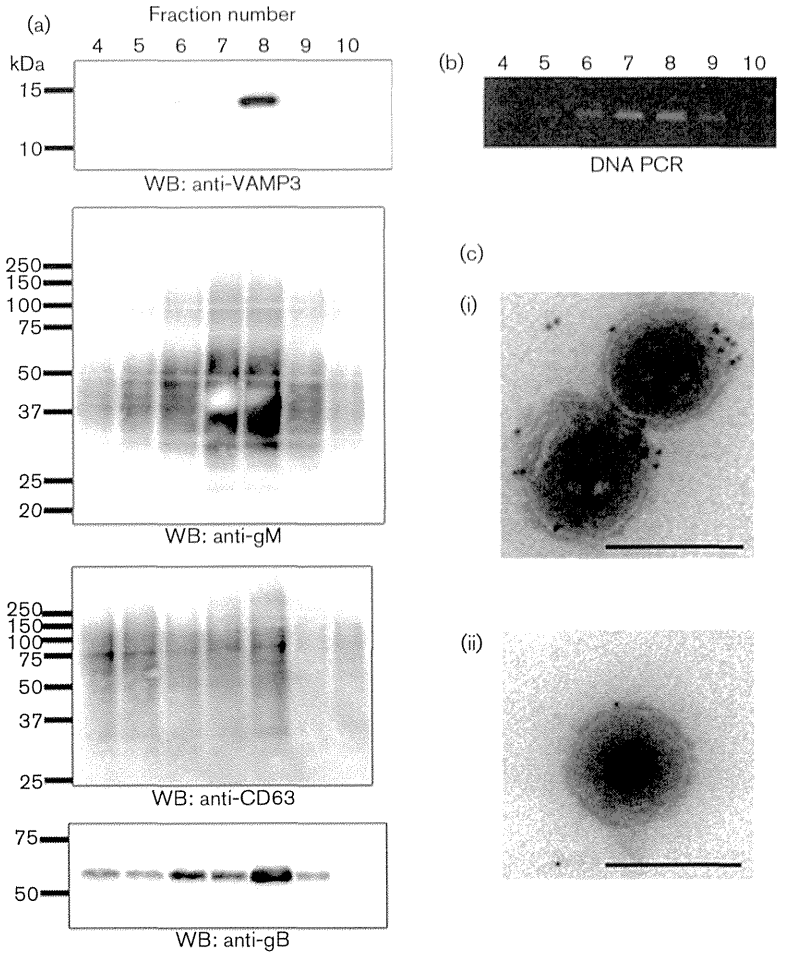

Fig. 4. The presence of VAMP3 in HHV-6A virions and exosomes. Exosome fractions containing virions were purified from the culture medium of HHV-6A-infected cells by sucrose density-gradient centrifugation and then analysed by Western blotting (a), DNA PCR (b) and electron microscopy (c). (a) Western blot analysis of the sucrose density-gradient fractions with anti-VAMP3, anti-gM, anti-CD63 or anti-gB Abs. (b) Viral DNA was detected in the fractions by PCR with HHV-6A specific primers. The numbers above the PCR image showed the fraction numbers. (c) Immunogold localization of VAMP3 on the HHV-6A virions. Purified virions (fraction 8) were labelled with antisera against VAMP3 (i) or without primary antibody (ii). Bars, 200 nm.

kidney cells (293T cells) and HeLa cells were cultured in Dulbecco's modified Eagle's medium supplemented with 8 % FBS. The HHV-6A strain GS was propagated and titrated in HSB-2 cells. HHV-6A cell-free virus was prepared as previously described (Akkapaiboon *et al.*, 2004). Cord blood mononuclear cells (CBMC) were used for virus propagation (Mori *et al.*, 2004). CBMCs were kindly provided by K. Adachi (Minoh Hospital, Minoh, Japan) and H. Yamada (Kobe University Graduate School of Medicine, Kobe, Japan) and purchased from the RIKEN Cell Bank (BioResource Center). For the usage of CBMCs, the study was approved by the ethics committee of each institution.

Antibodies. Rabbit antibody (Ab) specific for HHV-6A gM or gB (Mori *et al.*, 2008), an AgM-1 mAb against gM (Kawabata *et al.*, 2012), and a U14 mAb against HHV-6 U14 (Takemoto *et al.*, 2005) were used. mAbs against CD63 (clone CLB-gran/12, 435; Sanquin) and α-tubulin (clone B-5-1-2; Sigma), a sheep polyclonal Ab against TGN46 (AbD Serotec), a rabbit polyclonal Ab against VAMP3 (BioReagents) and a goat polyclonal Ab against VAMP3 (Santa Cruz) were used. Anti-HA (clone HA-7; Sigma) and anti-FLAG (clone M2; Sigma) antibodies were also used. Alexa Fluor 594-conjugated donkey anti-sheep IgG (Molecular Probes), Alexa Fluor 594-conjugated donkey anti-rabbit IgG (Molecular Probes), FITC-conjugated affinity pure $F(ab')_2$ fragment goat anti-guinea pig IgG (Jackson ImmunoResearch Laboratories), and Cy5-conjugated donkey anti-mouse IgG (Jackson ImmunoResearch Laboratories) were used as secondary antibodies. An anti-VAMP3 monospecific Ab was produced by subjecting guinea pigs to three rounds of immunization with the antigen, which was then expressed in *Escherichia coli* and purified (Mori *et al.*, 2008).

Immunofluorescence assay. The IFA was performed as described previously (Akkapaiboon *et al.*, 2004; Mori *et al.*, 2004). Specific immunofluorescence was observed under a confocal laser-scanning microscope (FluoView FV1000; Olympus).

Plasmid construction. The HA-tagged gM- and FLAG-tagged gN-expressing plasmids were described previously (Kawabata *et al.*, 2012). The pCAGGS plasmid was kindly provided by Jun-ichi Miyazaki (Osaka University, Japan) (Niwa *et al.*, 1991). To express the recombinant protein, the following primer pair was used to amplify inserts from HSB-2 cells cDNA: for named GST-VAMP3, VAMP3FbamHI (5′-ACCGGATCCTCTACAGGTCCAACTGCTGC-CACT-3′) and VAMP3rsalI (5′-ACCGTCGACTTACTTGCAATTCT-TCCACCAATATTTC-3′). The PCR products were inserted into the pGEX-4T1 vector (GE Healthcare).

Plasmid transfection. HeLa cells were transfected with the expression plasmids using Lipofectamine 2000 (Invitrogen) according to the manufacturer's instructions. The 293T cells were transfected using the calcium phosphate method as described previously (Koshizuka *et al.*, 2010).

Identification of gM/gN-interacting proteins. Plasmids expressing HA-tagged gM and FLAG-tagged gN were cotransfected into 293T cells. Cotransfection of gM and pCAGGS into 293T cells was performed as a control. At 72 h post-transfection, the cells were lysed in TNE buffer (0.01 M Tris/HCl, pH 7.4, 0.15 M NaCl, 1 mM EDTA, 1 % Nonidet-P-40). After centrifugation at 200 000 ***g*** for 1 h, the

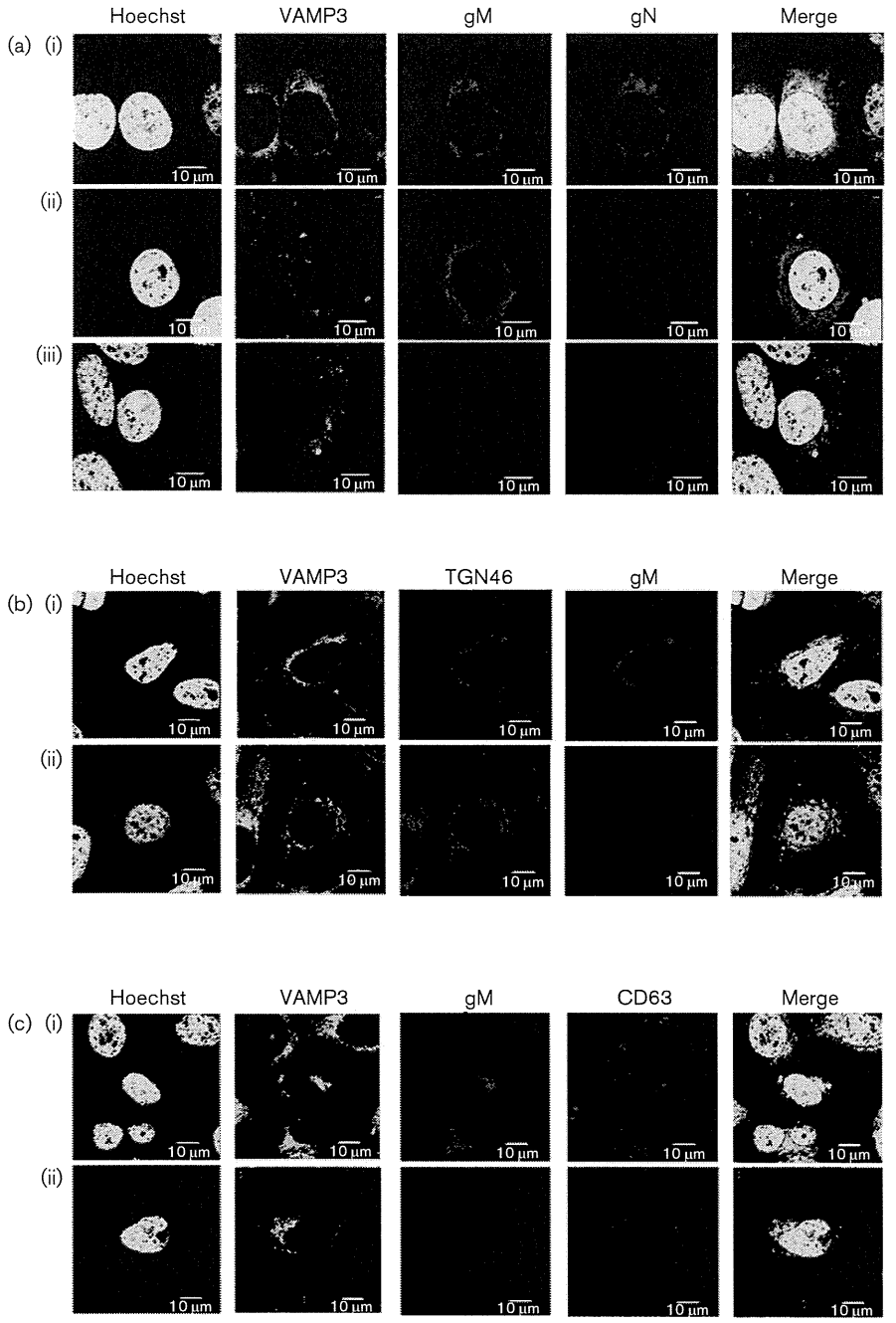

Fig. 5. Subcellular localization of VAMP3 with the gM/gN complex in HeLa cells transiently expressing gM and gN. HeLa cells were transfected with plasmids expressing gM and gN [a(i), b(i), c(i)], gM and the empty vector [a(ii)], or without vectors [a(iii), b(ii), c(ii)]. The cells were harvested at 48 h post-transfection and fixed. (a) The cells were stained with antibodies against gM, FLAG (for gN) and VAMP3 as well as with Hoechst 33258. (b) Cells were stained with antibodies against gM, TGN46 and VAMP3 as well as Hoechst 33258. (c) Cells were stained with antibodies against gM, CD63 and VAMP3 as well as with Hoechst 33258. Co-stained areas appear white or yellow in the merged panel. Bars, 10 μm.

supernatants were incubated overnight at 4 °C with an anti-HA antibody conjugated to protein G Sepharose (GE Healthcare). The protein-anti-HA conjugated beads were then washed with lysis buffer and the bound proteins were eluted with 0.1 M glycine/HCl (pH 2.8). After the beads were removed by centrifugation, the supernatants were neutralized by adding 1 M Tris-HCl (pH 9.5). The eluted proteins were then solubilized with sample buffer, separated on a NuPAGE SDS-PAGE system (Invitrogen), and examined by silver staining. Specific bands were analysed by LC-MS/MS to identify the coimmunoprecipitated proteins (Shevchenko *et al.*, 1996; Tang *et al.*, 2013).

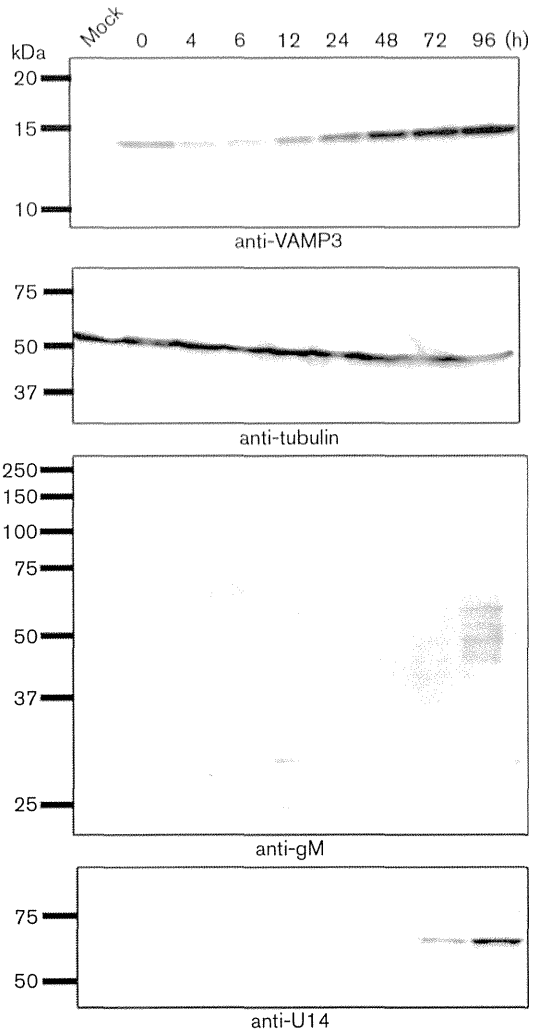

Fig. 6. Kinetics of VAMP3 protein expression in HHV-6A-infected cells. Whole-cell lysates collected at the indicated time points (h) were analysed by Western blotting. The numbers beside the panels indicate the molecular masses (kDa).

Western blotting. Western blotting was performed as described previously (Akkapaiboon *et al.*, 2004).

Isolation of virion fractions. Virions containing exosomes were collected from the cell culture medium by differential centrifugation and fractionated with a linear sucrose gradient, as described previously (Mori *et al.*, 2008). The fractions were analysed by Western blotting, DNA PCR, and electron microscopy.

Electron microscopy. Immunogold labelling of virions was performed as described previously (Mori *et al.*, 2008). The samples were examined under a Hitachi H-7650 electron microscope.

ACKNOWLEDGEMENTS

We thank E. Moriishi (National Institute of Biomedical Innovation), Mayuko Hayashi and Megumi Ota (Kobe University) for technical assistance, J. Miyazaki (Osaka University) for providing reagents, and K. Adachi (Minoh City Hospital) and H. Yamada (Kobe University) for the CBMCs. This work was supported by a Grant-in-Aid for Scientific Research (B) from the Japan Society for the Promotion of Science (JSPS).

REFERENCES

Ablashi, D. V., Balachandran, N., Josephs, S. F., Hung, C. L., Krueger, G. R., Kramarsky, B., Salahuddin, S. Z. & Gallo, R. C. (1991). Genomic polymorphism, growth properties, and immunologic variations in human herpesvirus-6 isolates. *Virology* **184**, 545–552.

Ablashi, D., Agut, H., Alvarez-Lafuente, R., Clark, D. A., Dewhurst, S., Diluca, D., Flamand, L., Frenkel, N., Gallo, R. & other authors (2014). Classification of HHV-6A and HHV-6B as distinct viruses. *Arch Virol* **159**, 863–870.

Akkapaiboon, P., Mori, Y., Sadaoka, T., Yonemoto, S. & Yamanishi, K. (2004). Intracellular processing of human herpesvirus 6 glycoproteins Q1 and Q2 into tetrameric complexes expressed on the viral envelope. *J Virol* **78**, 7969–7983.

Aubin, J. T., Collandre, H., Candotti, D., Ingrand, D., Rouzioux, C., Burgard, M., Richard, S., Huraux, J. M. & Agut, H. (1991). Several groups among human herpesvirus 6 strains can be distinguished by Southern blotting and polymerase chain reaction. *J Clin Microbiol* **29**, 367–372.

Baines, J. D. & Roizman, B. (1991). The open reading frames UL3, UL4, UL10, and UL16 are dispensable for the replication of herpes simplex virus 1 in cell culture. *J Virol* **65**, 938–944.

Borisovska, M., Zhao, Y., Tsytsyura, Y., Glyvuk, N., Takamori, S., Matti, U., Rettig, J., Südhof, T. & Bruns, D. (2005). v-SNAREs control exocytosis of vesicles from priming to fusion. *EMBO J* **24**, 2114–2126.

Campadelli-Fiume, G., Guerrini, S., Xiaoming, L. & Foà-Tomasi, L. (1993). Monoclonal antibodies to glycoprotein B differentiate human herpesvirus 6 into two clusters, variants A and B. *J Gen Virol* **74**, 2257–2262.

Chandran, B., Tirawatnapong, S., Pfeiffer, B. & Ablashi, D. V. (1992). Antigenic relationships among human herpesvirus-6 isolates. *J Med Virol* **37**, 247–254.

Dijkstra, J. M., Visser, N., Mettenleiter, T. C. & Klupp, B. G. (1996). Identification and characterization of pseudorabies virus glycoprotein gM as a nonessential virion component. *J Virol* **70**, 5684–5688.

Galli, T., Chilcote, T., Mundigl, O., Binz, T., Niemann, H. & De Camilli, P. (1994). Tetanus toxin-mediated cleavage of cellubrevin impairs exocytosis of transferrin receptor-containing vesicles in CHO cells. *J Cell Biol* **125**, 1015–1024.

Hobom, U., Brune, W., Messerle, M., Hahn, G. & Koszinowski, U. H. (2000). Fast screening procedures for random transposon libraries of cloned herpesvirus genomes: mutational analysis of human cytomegalovirus envelope glycoprotein genes. *J Virol* **74**, 7720–7729.

Hu, C., Hardee, D. & Minnear, F. (2007). Membrane fusion by VAMP3 and plasma membrane t-SNAREs. *Exp Cell Res* **313**, 3198–3209.

Jahn, R. & Scheller, R. H. (2006). SNAREs–engines for membrane fusion. *Nat Rev Mol Cell Biol* **7**, 631–643.

Jahn, R., Lang, T. & Südhof, T. C. (2003). Membrane fusion. *Cell* **112**, 519–533.

Kawabata, A., Jasirwan, C., Yamanishi, K. & Mori, Y. (2012). Human herpesvirus 6 glycoprotein M is essential for virus growth and requires glycoprotein N for its maturation. *Virology* **429**, 21–28.

Koshizuka, T., Ota, M., Yamanishi, K. & Mori, Y. (2010). Characterization of varicella-zoster virus-encoded ORF0 gene–comparison of parental and vaccine strains. *Virology* **405**, 280–288.

Krzyzaniak, M. A., Mach, M. & Britt, W. J. (2009). HCMV-encoded glycoprotein M (UL100) interacts with Rab11 effector protein FIP4. *Traffic* **10**, 1439–1457.

Lawrence, G. L., Nicholas, J. & Barrell, B. G. (1995). Human herpesvirus 6 (strain U1102) encodes homologues of the conserved herpesvirus glycoprotein gM and the alphaherpesvirus origin-binding protein. *J Gen Virol* **76**, 147–152.

Luftman, K., Hasan, N., Day, P., Hardee, D. & Hu, C. (2009). Silencing of VAMP3 inhibits cell migration and integrin-mediated adhesion. *Biochem Biophys Res Commun* **380**, 65–70.

McMahon, H. T., Ushkaryov, Y. A., Edelmann, L., Link, E., Binz, T., Niemann, H., Jahn, R. & Südhof, T. C. (1993). Cellubrevin is a ubiquitous tetanus-toxin substrate homologous to a putative synaptic vesicle fusion protein. *Nature* **364**, 346–349.

Mohrmann, R. & Sørensen, J. B. (2012). SNARE requirements en route to exocytosis: from many to few. *J Mol Neurosci* **48**, 387–394.

Mori, Y. (2009). Recent topics related to human herpesvirus 6 cell tropism. *Cell Microbiol* **11**, 1001–1006.

Mori, Y., Akkapaiboon, P., Yonemoto, S., Koike, M., Takemoto, M., Sadaoka, T., Sasamoto, Y., Konishi, S., Uchiyama, Y. & Yamanishi, K. (2004). Discovery of a second form of tripartite complex containing gH-gL of human herpesvirus 6 and observations on CD46. *J Virol* **78**, 4609–4616.

Mori, Y., Koike, M., Moriishi, E., Kawabata, A., Tang, H., Oyaizu, H., Uchiyama, Y. & Yamanishi, K. (2008). Human herpesvirus-6 induces MVB formation, and virus egress occurs by an exosomal release pathway. *Traffic* **9**, 1728–1742.

Niwa, H., Yamamura, K. & Miyazaki, J. (1991). Efficient selection for high-expression transfectants with a novel eukaryotic vector. *Gene* **108**, 193–199.

Osterrieder, N., Neubauer, A., Brandmuller, C., Braun, B., Kaaden, O. R. & Baines, J. D. (1996). The equine herpesvirus 1 glycoprotein gp21/22a, the herpes simplex virus type 1 gM homolog, is involved in virus penetration and cell-to-cell spread of virions. *J Virol* **70**, 4110–4115.

Polgár, J., Chung, S. H. & Reed, G. L. (2002). Vesicle-associated membrane protein 3 (VAMP-3) and VAMP-8 are present in human platelets and are required for granule secretion. *Blood* **100**, 1081–1083.

Roizmann, B., Desrosiers, R. C., Fleckenstein, B., Lopez, C., Minson, A. C., Studdert, M. J. & The Herpesvirus Study Group of the International Committee on Taxonomy of Viruses (1992). The family *Herpesviridae*: an update. *Arch Virol* **123**, 425–449.

Rothman, J. E. (1994). Mechanisms of intracellular protein transport. *Nature* **372**, 55–63.

Shevchenko, A., Wilm, M., Vorm, O. & Mann, M. (1996). Mass spectrometric sequencing of proteins silver-stained polyacrylamide gels. *Anal Chem* **68**, 850–858.

Söllner, T., Whiteheart, S. W., Brunner, M., Erdjument-Bromage, H., Geromanos, S., Tempst, P. & Rothman, J. E. (1993). SNAP receptors implicated in vesicle targeting and fusion. *Nature* **362**, 318–324.

Takemoto, M., Koike, M., Mori, Y., Yonemoto, S., Sasamoto, Y., Kondo, K., Uchiyama, Y. & Yamanishi, K. (2005). Human herpesvirus 6 open reading frame U14 protein and cellular p53 interact with each other and are contained in the virion. *J Virol* **79**, 13037–13046.

Tang, H., Serada, S., Kawabata, A., Ota, M., Hayashi, E., Naka, T., Yamanishi, K. & Mori, Y. (2013). CD134 is a cellular receptor specific for human herpesvirus-6B entry. *Proc Natl Acad Sci U S A* **110**, 9096–9099.

Tayeb, M. A., Skalski, M., Cha, M. C., Kean, M. J., Scaife, M. & Coppolino, M. G. (2005). Inhibition of SNARE-mediated membrane traffic impairs cell migration. *Exp Cell Res* **305**, 63–73.

Tischer, B. K., Schumacher, D., Messerle, M., Wagner, M. & Osterrieder, N. (2002). The products of the UL10 (gM) and the UL49.5 genes of Marek's disease virus serotype 1 are essential for virus growth in cultured cells. *J Gen Virol* **83**, 997–1003.

Veale, K. J., Offenhäuser, C., Lei, N., Stanley, A. C., Stow, J. L. & Murray, R. Z. (2011). VAMP3 regulates podosome organisation in macrophages and together with Stx4/SNAP23 mediates adhesion, cell spreading and persistent migration. *Exp Cell Res* **317**, 1817–1829.

Yamagishi, Y., Sadaoka, T., Yoshii, H., Somboonthum, P., Imazawa, T., Nagaike, K., Ozono, K., Yamanishi, K. & Mori, Y. (2008). Varicella-zoster virus glycoprotein M homolog is glycosylated, is expressed on the viral envelope, and functions in virus cell-to-cell spread. *J Virol* **82**, 795–804.

Yamanishi, K., Shiraki, K., Kondo, T., Okuno, T., Takahashi, M., Asano, Y. & Kurata, T. (1988). Identification of human herpesvirus-6 as a causal agent for exanthem subitum. *Lancet* **331**, 1065–1067.

Journal of proteome research

Article

pubs.acs.org/jpr

Identification of Sialylated Glycoproteins in Doxorubicin-Treated Hepatoma Cells with Glycoproteomic Analyses

Kanako Azuma,[†] Satoshi Serada,[‡] Shinji Takamatsu,[†] Naoko Terao,[†] Shunsaku Takeishi,[§] Yoshihiro Kamada,[†] Tetsuji Naka,[‡] and Eiji Miyoshi*[,†]

[†]Department of Molecular Biochemistry & Clinical Investigation, Osaka University Graduate School of Medicine, Osaka 565-0871, Japan

[‡]Laboratory for Immune Signal, National Institute of Biomedical Innovation, Osaka 567-0085, Japan

[§]Department of Gastroenterology and Oncology, Institute of Health Biosciences, The University of Tokushima Graduate School, Tokushima 770-0855, Japan

S *Supporting Information*

ABSTRACT: Sialylation is one of the most important types of glycosylation involved in carcinogenesis and establishment of cancer stemness. We previously showed that increased sialylation is a characteristic glycan change in cancer stem cells (CSCs) from hepatocellular carcinoma. However, the identities of glycoproteins targeted for sialylation remain unknown. In the present study, we identified glycoproteins targeted for sialylation in doxorubicin (DXR)-treated hepatocarcinoma cell line, Huh7, using glycoproteomic analyses. Since CSCs constitute a small subset of cells within carcinoma cell lines, it is difficult to identify sialylated proteins using general glycoproteomic strategies. It is known that treatment with anticancer drug can condense CSCs, we used DXR to concentrate CSCs. In DXR-treated Huh7 cells, isobaric tag for relative and absolute quantitation (iTRAQ) analysis identified 17 sialylated glycoproteins. Most of the identified glycoproteins were cancer-associated proteins. Furthermore, two proteins of approximately 70 kDa were detected using *Sambucus sieboldoana* agglutinin (SSA) blot analysis and identified as beta-galactosidase and alpha-2-HS-glycoprotein (fetuin-A) by SSA precipitation followed by liquid chromatography-tandem mass spectrometry analyses. Sialylation levels of fetuin-A were increased in DXR-treated Huh7 cell lysates. These changes in sialylation of glycoproteins might be involved in the establishment of cancer stemness.

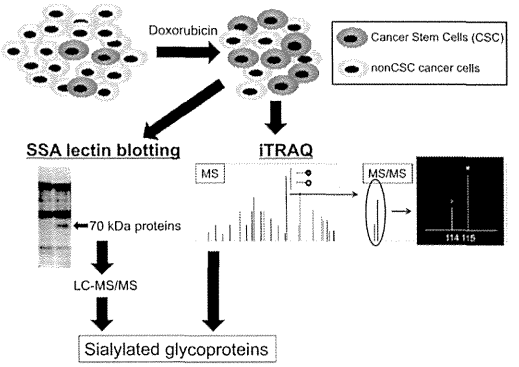

KEYWORDS: *sialylation, cancer stem cells, doxorubicin, hepatoma, glycoproteomics*

INTRODUCTION

A growing body of evidence suggests that tumors are frequently composed of heterogeneous cell types and that tumor initiation and growth are driven by a small subset of cells, termed cancer stem cells (CSCs), or tumor-initiating cells.[1−3] Several lines of research have indicated that CSCs can be preferentially resistant to many current therapies, including various chemotherapeutic agents and radiation treatment.[4−7] Thus, therapeutic strategies that effectively target CSCs could have a major impact on cancer patient survival. There are many reports on CSC markers, which include CD13,[8] CD44,[9,10] epithelial cell adhesion molecule (EpCAM),[11] and CD133.[9,12,13] These CSC markers have been used for identifying or concentrating CSCs in each type of cancer. It is unknown whether pure CSCs or whether heterogeneous populations containing CSC-like cells, should be targets for therapeutic strategies. Glycans are often attached to proteins and lipids on the cell surface and structurally and functionally modify these molecules. Glycans consist of several kinds of monosaccharides and show great structural diversity. Research in the field of glycobiology has revealed diverse and complex biological roles for these glycans.[14] The structures and amounts of glycans present on the cell surface change dramatically during development and differentiation.[15] We have recently reported that sialylated glycans are useful markers for CSC-like cells in hepatoma cell lines.[16] Glycomic analysis using a lectin microarray showed marked binding of *Sambucus sieboldoana* agglutinin (SSA) to a $CD133^{+}CD13^{+}$ cell subpopulation within hepatoma cell lines. SSA lectin recognizes $\alpha 2$, 6-sialic acid.[16] Sialic acid is one of the building blocks of glycans and is generally found at the outermost ends of the glycan chains of glycoproteins and glycolipids. Thus, sialic acid is associated with many physiological and pathological events, including binding to infectious pathogens, regulation of immune responses, and tumor malignancy.[17] In particular, the alteration of sialic acid moieties is associated with cancer cell behavior, such as invasiveness and metastasis.[18−23] Glycan changes are involved in development and differentiation, and sialic acid is one of the most important glycosylations involved in these processes.[24]

Special Issue: Proteomics of Human Diseases: Pathogenesis, Diagnosis, Prognosis, and Treatment

Received: May 1, 2014
Published: August 26, 2014

ACS Publications © 2014 American Chemical Society

In terms of glycoproteomic analyses, the identification of target proteins for each characteristic oligosaccharide structure is very important.[25] However, using the conventional strategy, which involves pooling and concentrating the CSC fraction using CD markers and lectins, it was not easy to obtain appropriate amounts of proteins for glycomic analyses. In general, CSC or CSC-like cells are resistant to anticancer drug treatment. For example, a CD133 and SSA double-positive population was resistant to several kinds of anticancer drug treatments such as 5-fluorouracil (5-FU) (Supplementary Figure 1). Hermann et al. also showed that the number of CD133-positive cells increased in human pancreatic cancer cells treated with gemcitabine.[26] These results suggest that short-term treatment with anticancer drugs can be used to easily concentrate CSCs. Among emerging proteomic technologies, isobaric tags for relative and absolute quantitation (iTRAQ) is a shotgun-based technique, which allows the concurrent identification and relative quantification of hundreds of proteins from different biological samples in a single experiment.[27,28] Whereas iTRAQ analysis leads to a more comprehensive analysis of sialylated proteins, the SSA lectin precipitation technique followed by liquid chromatography–tandem mass spectrometry (LC–MS/MS) analysis allows for protein enrichment, which aids in the identification of specific target proteins.

In the present study, we investigated characteristic glycan structures in the doxorubicin (DXR)-treated human hepatoma cell line Huh7, and further identified their target glycoproteins using iTRAQ and SSA lectin precipitation followed by LC–MS/MS. In addition, the expression levels of these proteins were confirmed using Western blotting, and their biological significance in CSC functions is discussed.

MATERIALS AND METHODS

Cell Culture and Cell Treatments

The human hepatoma cell line Huh7 was obtained from American Type Culture Collection (ATCC, Manassas, VA, USA) and cultured in RPMI 1640 (Sigma, St. Louis, MO, USA) medium containing 10% fetal bovine serum (Invitrogen, Carlsbad, CA, USA), supplemented with 100 units/mL penicillin G and 100 μg/mL streptomycin in a 37 °C incubator under a humidified atmosphere containing 5% CO_2. The cells were seeded into 100 mm dishes at 1×10^6 cells/dish. After 6 h, doxorubicin (DXR) (Sigma) was added to the culture medium (5 μg/mL). The cells were harvested after 48 h of exposure to DXR, and the culture media were harvested as conditioned media for the following analyses.

Lectin Microarray

Patterns of oligosaccharide structures in Huh7 cells treated with or without DXR were investigated by means of evanescent-field fluorescence-assisted lectin microarray. Forty-five types of lectins were immobilized on a glass slide in triplicate. The procedure has been described in detail, previously.[29] Briefly, total cellular proteins in phosphate buffered saline (PBS) containing 1% Triton X-100 were labeled with Cy3-succinimidyl ester (GE Healthcare, Chalfont St. Giles, U.K.) at room temperature (RT) for 1 h in the dark. Excess reagent was removed by gel filtration chromatography. The resultant Cy3-labeled protein solution was applied to a lectin microarray. After incubation at 20 °C for 15 h, the glass slide was scanned with an evanescent-field fluorescence scanner, GlycoStation (GP Biosciences Ltd., Kanagawa, Japan). All of the data were analyzed using Array Pro Analyzer version 4.5 (Media Cybernetics, Inc., Bethesda, MD, USA). The net intensity value for each spot was calculated by subtracting the background value. The signal intensity value for each lectin was expressed as the average of the net intensity values for three spots. The signal from wheat germ agglutinin (WGA) was used to normalize the signal intensity of each lectin because binding to WGA lectin was relatively stable and similar using different cell types.

Mass Spectrometric Analysis

NanoLC–MS/MS analyses were performed on LTQ-Orbitrap XL (Thermo Fisher Scientific, Waltham, MA) equipped with nano-ESI source and coupled to Paradigm MG4 pump (Michrom Bioresources, Auburn, CA) and autosampler (HTC PAL, CTC Analytics, Zwingen, Switzerland). Peptide mixtures were separated on MagicC18AQ column (100 mm × 150 mm, 3.0 μm particle size, 300 Å, Michrom Bioresources) with a flow rate of 500 nL/min. A linear gradient of 5–30% B in 80 min, 30–95% B in 10 min, and 95% B for 4 min and finally decreased to 5% B was employed (A = 0.1% formic acid in 2% acetonitrile; B = 0.1% formic acid in 90% acetonitrile). Intact peptides were detected in the Orbitrap at 30,000 resolution. Up to three CID and HCD spectra were acquired in a data-dependent acquisition mode following each full scan (m/z, 400–1500). The mass spectrometer was operated in positive ion mode.

Preparation of Labeled Peptides for Isobaric Tags for Relative and Absolute Quantitation (iTRAQ) Analysis

Each protein sample (adjusted to 4.1 mg) was digested with 50 μg of Trypsin-TPCK Solution (Applied Biosystems, Framingham, MA, USA) at 37 °C overnight and sialylated proteins were isolated using *Sambucus sieboldiana* agglutinin (SSA) covalently linked to agarose beads (SSA-agarose) (J-Oil Mills, Inc., Tokyo, Japan). After applying to an SSA-agarose column, each sample was incubated for 6 h at 4 °C. The SSA-Agarose column was washed with 1 mL of 50 mM Tris HCl [pH 7.4] buffer five times. Bound peptides were eluted from the SSA-Agarose column using 1 mL of the elution buffer (0.2 M lactose) three times. The eluted samples were deglycosylated with glycopeptidase F. Deglycosylated peptides were desalted and labeled with iTRAQ reagents (Applied Biosystems) according to the manufacturer's instructions. Proteins from Huh7 cells, treated with or without DXR and eluted from SSA agarose, were labeled with iTRAQ reagents 114 and 115, respectively. All labeled peptide samples were mixed and fractionated as described previously.[30]

iTRAQ Data Analysis

Protein identification and quantification for iTRAQ analysis was carried out using Proteome Discoverer v.1.3 (Thermo Fisher Scientific) using the MASCOT algorithm against Swiss-Prot protein database (Swiss-Prot_2012_06 536,489 entries). Taxonomy was set to *Homo sapiens* (20,312 entries). Search parameters for peptide and MS/MS mass tolerance were 10 ppm and 0.8 Da, respectively, with allowance for two missed cleavages made from the trypsin digest. Carbamidomethylation (Cys) and iTRAQ4plex (Lys, N-terminal) were specified as static modifications, whereas deamidation (Asn, Gln), iTRAQ4plex (Tyr), and oxidation (Met) were specified as dynamic modifications in the database search. When deamidation of Asn were detected, the amino acids were considered as glycan binding site because glycopeptidase F treatment convert glycosylated Asn residue to Asp. Mascot results were filtered with the integrated Percolator based filter using a false discovery rate <1% (based on PSMs). Relative protein abundances were calculated using the ratio of iTRAQ reporter ion in the MS/MS scan. List of the

glycoproteins identified in iTRAQ analysis was represented in Supplementary Table 1.

Protein Identification by Mass Spectrometry

The gels were stained with the Silver Stain MS kit according to the manufacturer's instruction (WAKO Pure Chemical Industries, Ltd., Osaka, Japan). Protein spots in a silver-stained gel, corresponding to positive spots on Western blot membranes, were excised from the gel and digested in gel according to a previously described method,[31,32] using sequencing grade modified trypsin (Promega, Inc., Madison, WI). Digested peptides were then extracted with 5% TFA in acetonitrile (acetonitrile/DW 50:45), sonicated for 5 min and concentrated by evaporation. Dried peptides were dissolved in 0.1% TFA (v/v) and 2% acetonitrile (v/v) for subsequent LC–MS/MS analysis. NanoLC–MS/MS analyses were performed on a LTQ-Orbitrap XL mass spectrometer (Thermo Fisher Scientific) equipped with a nano-ESI source (AMR) and coupled to a Paradigm MG4 pump (Michrom Bioresources) and an autosampler (HTC PAL, CTC Analytics). A spray voltage of 1800 V was applied. The peptide mixture was separated on a Magic C18AQ column (100 μm × 150 mm, 3.0 μm particle size, 300 Å, Michrom Bioresources) with a flow rate of 500 nL/min. The linear gradient of 5% to 45% B in 30 min, 45% to 95% B in 0.1 min, and 95% B for 2 min and finally decreased to 5% B was employed (A = 0.1% formic acid in 2% acetonitrile; B = 0.1% formic acid in 90% acetonitrile). Intact peptides were detected in the Orbitrap at 60,000 resolutions. For LC–MS/MS analysis, 6 precursor ions were selected for subsequent MS/MS scans in a data-dependent acquisition mode following each full scan (m/z, 350–1500). A lock mass function was used for the LTQ-Orbitrap to obtain constant mass accuracy during gradient analysis. Peptides and proteins were identified by means of automated database search using Proteome Discoverer v.1.3 (Thermo Fisher Scientific) against human of Swiss-Prot protein database (Swiss-Prot_2012_06) with a precursor mass tolerance of 10 ppm, a fragment ion mass tolerance of 0.8 Da, and strict trypsin specificity, allowing for up to two missed cleavages. Carbamidomethylation of cysteine was set as a fixed modification, and oxidation of methionines was allowed as dynamic modifications. Raw data of MS/MS analysis was represented in Supplementary Figure 2.

Lectin Blot Analysis

Huh7 cells were quickly harvested from a 100 mm dish in ice-cold PBS. After precipitation by centrifugation at 2000 rpm for 5 min at 4 °C, the cells were resuspended in TNE buffer (10 mM Tris-HCl [pH 7.8], 1% NP40, 1 mM EDTA, and 0.15 M NaCl) containing a protease inhibitor cocktail (Roche, Mannheim, Germany) and then placed on ice for 30 min to allow solubilization. Samples were then centrifuged at 15,000 rpm for 15 min at 4 °C, and the supernatants were collected as cell lysates. Samples were quantitated using a bicinchoninic acid (BCA) assay kit (Pierce, Rockford, IL, USA).

In each experiment, duplicate samples were subjected to 8% sodium dodecyl sulfate polyacrylamide gel electrophoresis (SDS-PAGE) under reducing conditions. One gel was subjected to Coomassie Brilliant Blue (CBB) R-250 staining and another was transferred to a polyvinyl difluoride (PVDF) membrane (Millipore Corp., Billerica, MA, USA) for lectin blot analysis, using SSA, *Leukoagglutinating phytohemagglutinin* (L4-PHA), *Aleuria aurantia* lectin (AAL), and *Datura stramonium* (DSA). After blocking with PBS containing 3% bovine serum albumin (BSA) overnight at 4 °C, each membrane was incubated in 1:2500–1:10000 diluted biotinylated SSA, L4-PHA, AAL, and DSA (J-Oil Mills, Inc., Tokyo, Japan) for 20 min at RT. The membranes were then washed three times with Tris-buffered saline containing 0.05% Tween-20 (TBST) (pH 7.4) and incubated with 1:2500 diluted avidin–peroxidase conjugates (ABC kits, Vector Res. Corp., Burlingame, CA, USA) for 20 min at RT. The membrane was again washed three times with TBST and then developed using an enhanced chemiluminescence system, Immobilon Western (Millipore), according to the manufacturer's protocol.

Immunoblot Analysis

Cell lysates and conditioned media were subjected to 8% SDS-PAGE under reducing conditions and then transferred to a PVDF membrane (Millipore). After blocking with PBS containing 5% skim milk for 1 h at RT, each membrane was incubated overnight at 4 °C with the following primary antibodies diluted 1:1000–1:5000: anti-HYOU1 (Abnova, Taipei, Taiwan), anti-P4HA1 (Abnova, Taipei City, Taiwan), anti-LAMP1 (Abcam Inc., Cambridge, MA, USA), anti-LAMP2 (Santa Cruz Biotechnology Inc., Santa Cruz, CA, USA), antibeta-galactosidase (Santa Cruz Biotechnology), antifetuin-A (Santa Cruz Biotechnology), or anti-β-actin (Cell Signaling, Beverly, MA, USA) for 60 min at RT. The dilution ratios for these antibodies ranged from 1:1000 to 1:5000. The membranes were then washed three times with Tris-buffered saline containing 0.05% Tween-20 (TBST) (pH 7.4) and incubated with 1:5000 diluted horseradish peroxidase conjugated with the appropriate secondary antibody for 30 min at RT. The membranes were again washed three times and developed using an Immobilon Western (Millipore).

Lectin Precipitation

Extracted protein (100 μg) was incubated with 40 μL of SSA-agarose overnight with shaking at 4 °C. Precipitated proteins were washed in 50 mM Tris HCl [pH 7.4] and then boiled in SDS sample buffer. Ten microliters of precipitated proteins were subjected to 8% SDS-PAGE. The gel was stained with Silver Stain MS Kits (Wako, Osaka, Japan). Protein bands were excised from the gel and digested with sequencing grade trypsin (Promega) as described previously.[33]

Neuraminidase/*N*-Glycanase Treatments

The extracted proteins (100 μg) were incubated overnight at 37 °C with 200 mU/mL of neuraminidase (Roche, Nutley, NJ, USA) in 50 mM AcOH buffer [pH 5.5] containing 4 mM $CaCl_2$ and 100 μg/mL BSA. In addition, 100 μg of the extracted proteins were incubated with glycopeptidase F (Takara Bio Inc., Otsu, Japan) according to the manufacturer's protocol. The cell lysates were subsequently boiled in SDS-PAGE sample buffer, electrophoresed on 8% SDS PAGE, and then transferred onto a PVDF membrane (Millipore). After blocking with TBST containing 5% skim milk at 4 °C overnight, Western blot analysis for fetuin-A was performed using antifetuin-A antibody.[34] Briefly, 1:5000 diluted antifetuin-A was incubated in TBST buffer containing 5% skim milk for 1 h at RT. After washing the membrane three times with TBST, it was incubated for 1 h at RT with the secondary antibody, horseradish peroxidase-conjugated antirabbit-IgG (Promega), diluted 1:5000. It was again washed three times and developed with an Immobilon Western (Millipore).

Immunofluorescence Confocal Microscopy

Huh7 cells were seeded in 35 mm dishes at 3×10^5 cells/dish. After 6 h, DXR was added to the culture medium (5 μg/mL). After 48 h of exposure to DXR, cells were washed once in PBS